LASER MARKSMANSHIP POTENTIAL EVALUATION: MATH MODELING AND EXPERIMENTAL VERIFICATION

by
Ronald L. Phillips
Larry C. Andrews

FINAL REPORT

PREPARED FOR

U.S. ARMY PROJECT MANAGER FOR TRAINING DEVICES
located at
NAVAL TRAINING EQUIPMENT CENTER (NTEC)
ORLANDO, FLORIDA 32813

by

ENGINEERING AND INDUSTRIAL EXPERIMENT STATION
COLLEGE OF ENGINEERING
UNIVERSITY OF CENTRAL FLORIDA

JULY 1980

DISCLAIMER

The contents of this publication are not to be construed as an official Department of the Army position, unless so designated by other authorized documents.

Citation of manufacturer's or trade names does not institute an official endorsement or approval of the use thereof.

Destroy this report when no longer needed. Do not return it to the originator.

SECURITY CLASSIFICATION OF THIS PAGE (When Data Entered)

REPORT DOCUMENTATION PAGE

READ INSTRUCTIONS BEFORE COMPLETING FORM

1. REPORT NUMBER: PM TRADE - SE-0006	2. GOVT ACCESSION NO.: AD-A104 458
3. RECIPIENT'S CATALOG NUMBER:	
4. TITLE (and Subtitle): Laser Marksmanship Potential Evaluation: Math Modelling and Experimental Verification	5. TYPE OF REPORT & PERIOD COVERED: Final Report
	6. PERFORMING ORG. REPORT NUMBER:
7. AUTHOR(s): Dr. Ronald L. Phillips; Dr. Larry C. Andrews	8. CONTRACT OR GRANT NUMBER(s): N61339-79-D-0105 DO 0027
9. PERFORMING ORGANIZATION NAME AND ADDRESS: Engineering & Industrial Experiment Station, College of Engineering, University of Central Florida, Orlando, Fla. 32816	10. PROGRAM ELEMENT, PROJECT, TASK AREA & WORK UNIT NUMBERS: 62727A230
11. CONTROLLING OFFICE NAME AND ADDRESS: US Army (DRCPM-TND-RE) Project Manager for Training Devices, United States Army, Orlando, Florida 32813 305-646-5771	12. REPORT DATE: July 1980
	13. NUMBER OF PAGES: 90
14. MONITORING AGENCY NAME & ADDRESS (If different from Controlling Office)	15. SECURITY CLASS. (of this report): Unclassified
	15a. DECLASSIFICATION/DOWNGRADING SCHEDULE

16. DISTRIBUTION STATEMENT (of this Report)

Approved for public release; distribution unlimited

17. DISTRIBUTION STATEMENT (of the abstract entered in Block 20, if different from Report)

18. SUPPLEMENTARY NOTES

19. KEY WORDS (Continue on reverse side if necessary and identify by block number)

Trainer	MILES	Propagation	Lognormal
Weapons	Decoding	Probability	K-distribution
Tactical	Atmosphere	Moments	Turbulence
Laser	Model	Scintillation	

20. ABSTRACT (Continue on reverse side if necessary and identify by block number)

An analysis of the potential of using MILES systems for long range gunnery training was performed. The analysis centered on the evaluation of the design equations used for the MILES system design. Experiments were conducted at Kennedy Space Center which showed the MILES propagation equations to be accurate at only short ranges i.e. for distances only up to 180 meteres. New math models were developed for the propagation of laser light over the long ranges which would be used in gunnery training. These math models were verified in the Kennedy Space Center experiments.

DD FORM 1 JAN 73 1473 EDITION OF 1 NOV 65 IS OBSOLETE
S/N 0102-014-6601

SECURITY CLASSIFICATION OF THIS PAGE (When Data Entered)

An acurate analysis was also performed on the decoding technique of Binary Union Decoding used in the MILES system. This decoding technique was designed to defeat the laser signal fading effects of atmospheric turbulence. At long ranges the Binary Union Decoding technique proved to be less effective than at short ranges.

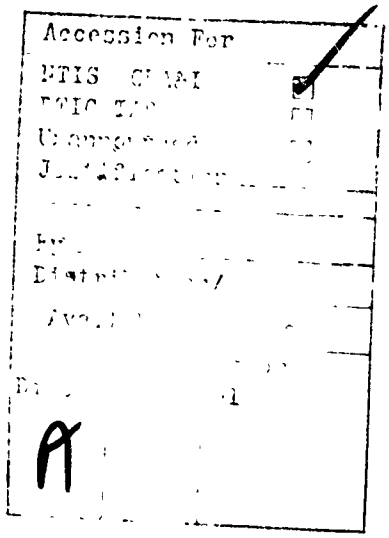

ACKNOWLEDGEMENT

The authors wish to thank Mr. Art Weeks and Mr. Madjid Belkerdid who both worked long hours on this project. Also we would like to thank Mr. David Douglas who developed many unique and creative electronic circuits used in the experimental portion of the project. We are also undebted to the officials of Kennedy Space Center and to the Manager of the Space Shuttle Landing Faculty, Mr. Billie L. Study, for their cooperation during our experiments at the Shuttle Landing Faculty.

TABLE OF CONTENTS

I. INTRODUCTION

The MILES system was designed and built as a tactical laser weapon fire simulator (LWFS). All of the mathematical analysis and experiments performed during the Advanced Development (AD) phase were to show that MILES would accurately simulate tactical weapon fire. The use of MILES for long range marksmanship gunnery training will require the kill zone of the MILES transmitter to be very narrow and well defined. It is the purpose of this study to construct mathematical models for long range laser propagation which will permit evaluation of the MILES equipment for marksmanship gunnery training. The study also includes an accurate analysis of the Binary Union decoder used in the MILES receiver. The Binary Union decoder was designed to increase the detection probability of received MILES words under very specific fading conditions. The currently available analysis makes several assumptions that are compatible with the short range problem, but for long ranges a more accurate analysis is required, for if the short range (200 meters) analysis were to be extended to the longer ranges an overly optimistic system performance results.

A. Background:

It has long been recognized that an optical beam propagating only several meters through clear-air turbulence will result in a redistribution of its energy, leading to fluctuations in the beam intensity commonly referred to as "scintillations". The statistics associated with these scintillations have been the subject of many theoretical and experimental investigations [1] - [12]. Much of the theoretical work dealt with approximation schemes for the solution of the wave equation describing the propagation of an optical beam through a

turbulent atmosphere. While these approximations have led to several different theoretical descriptions for the intensity fluctuations, the lognormal model has been more commonly accepted than the others. For propagation paths up to around 200 meters (or under conditions of weak turbulence) the logarithm of the intensity of the distorted wave is assumed to be normally distributed; hence the intensity itself is said to have a lognormal distribution. A large number of measurements have been made over the years which tend to support the lognormal model in the weak turbulence regime [9] - [12].

For distances beyond 200 meters (or under conditions of strong turbulence) the probability density function (pdf) associated with the optical scintillations is still a matter of great controversy. Several different models have been proposed for this saturation regime where multiple scattering effects are prominent. These models range from perturbed forms of the lognormal distribution [13], [14], to the K-distribution [6], [9]. Although the K-distribution provides reasonably accurate predictions for the statistical moments in part of the saturation regime, it is not theoretically applicable in areas of weak scattering where the mean-square fluctuation $\langle I^2 \rangle / \langle I \rangle^2$ falls below 2

A new mathematical model is proposed here which we believe is applicable for all propagation path lengths and conditions of turbulence. The model takes into account both the specular component of the optical beam and the diffuse component(s) which begin to be prominent when multiple scattering effects are important. We believe the reason the lognormal model fails to accurately describe the phenomenon in the saturation regime is that it ignores the diffuse component(s) of the beam. Owing to the presence of both of these components of the beam,

the proposed model has characteristics of the lognormal distribution over short propagation paths while approaching the negative exponential distribution as the propagation path tends to infinity. Recent measurements made by Parry and Pusey [9], as well as our own measurements over propagation paths from 200 - 3000 meters, tend to support this new mathematical model.

II. ATMOSPHERIC MODEL

Optical communication systems operating in a clear-air atmosphere are subject to many variations in atmospheric conditions. To study such systems in general would require a very complex model of the atmosphere. Frequently it is the case that the particular phenomenon of interest of the optical system may be the result of only certain atmospheric variations and other atmospheric conditions can be reasonably ignored. This appears to be the case in studying the intensity scintillations associated with an optical beam traversing a clear-air atmosphere.

A. The Refractive-Index Structure Parameter:

One of the most significant parameters of the atmosphere for optical propagation is the index of refraction. At a point $\underset{\sim}{r}$ in space and time t the index of refraction can be mathematically expressed by

$$n(\underset{\sim}{r},t) = n_o + n_1(\underset{\sim}{r},t), \qquad (2.1)$$

where $n_0 = \langle n(\underset{\sim}{r},t)\rangle$ is the average value over some continuously monitored time period and n_1 represents the random deviation of n from its average value.

For optical frequency signals the refractive-index fluctuations are caused almost exclusively by atmospheric temperature variations. These atmospheric temperature fluctuations originate primarily from the heating of the earth's surface, but then these variations are further broken and mixed by the wind which gives rise to a continuum of different scale sizes. This leads to the refracture-index being proportional to the temperature fluctuations

Since the time period associated with transmitting a laser beam is of the order of a few minutes or less, we will be interested in refractive-index fluctuations over similar time periods. Thus we can assume the "frozen-in" turbulence model wherein the index fluctuations at a point are generated by different sized "blobs", or turbulent eddies, swept past the point by the mean wind. With this model we need consider only the spatial structure of the turbulence so that (2.1) can be rewritten as

$$n(\underset{\sim}{r}) = n_o + n_1(\underset{\sim}{r}). \tag{2.2}$$

The turbulent eddies have a lens-like effect on an optical beam propagating through the atmosphere [4]. These eddies vary in size from ℓ_o, a scale of only a few millimeters and called the inner scale of turbulence, to an outer scale denoted by L_o. When the propagating beam is near the ground the dimension of L_o is roughly comparable with the beam height above the ground. These different sized eddies are responsible for both diffractive and refractive effects on the optical beam, which results in both constructive and destructive interference of the beam. It is the interplay of refractive-optical phase shift and diffractive-optical ray bending of the light rays that account for the observed amplitude fluctuations, and hence, intensity fluctuations.

Assuming spatial stationarity and homogeneity of the atmosphere, we define the autocovariance function and spatial power spectrum of the refractive-index fluctuations by [2]

$$B_n(r) = \langle n_1(r_1) n_1(r_1 + r) \rangle$$

$$= \frac{4\pi}{r} \int_0^\infty \Phi_n(k) k \sin(kr)\, dk \qquad (2.3)$$

and

$$\Phi_n(k) = \frac{1}{2\pi^2 k} \int_0^\infty B_n(r) r \sin(kr)\, dr, \qquad (2.4)$$

which are three-dimensional Fourier transforms of each other. Because of radial symmetry, the integrals reduce to a single integral in terms of the radial variable r and spatial wave number k.

Tartarski [1] suggested that the power spectrum had the same form as the wind velocity spectrum, viz.,

$$\Phi_n(k) = 0.033\, C_n^2\, k^{-11/3} \exp(-k^2/k_m^2), \qquad (2.5)$$

where $k_m = 5.92/\ell_o$. The refractive-index structure parameter C_n^2 is a measure of the intensity of the refractive-index fluctuations (i.e., a measure of the intensity of the turbulence). Although it is often referred to as the structure "constant", it typically ranges in values from 10^{-17} or less, for conditions of weak turbulence, up to 10^{-13} or more when the turbulence is strong. Over short time intervals at a fixed distance, for a constant height of the propagation path above the ground, it is reasonable to assume C_n^2 is essentially constant.

Eq. (2.5) is accepted as valid only for small scales such that $k > k_m$. For large scales such that $k < k_o$, where $k_o = 2\pi/L_o$, the approximation is poor. A better approximation for $\Phi_n(k)$ in this latter case is given by [7]

$$\Phi_n(k) = 0.033\, C_n^2\, (k^2 + 1/L_o)^{-11/6}\ \exp(-k^2/k_m^2), \qquad (2.6)$$

called the modified von Karman spectrum.

III. OPTICAL INTENSITY FLUCTUATIONS

In this section we describe several of the parameters of interest in optical scintillations such as log-amplitude, log-intensity, normalized variance, and log-intensity variance. Connecting relations between these terms and the lognormal model are discussed so as to present a background for the math model developed in Section V.

In the absence of turbulence the field of an optical beam can be expressed mathematically by

$$U_o(t) = A_o e^{i\omega t}, \tag{3.1}$$

where A_o is the (constant) amplitude of the field, ω is the angular frequency of the wave, and $i = \sqrt{-1}$. The incident intensity of the undisturbed field is then

$$I_o = |U_o(t)|^2 = A_o^2. \tag{3.2}$$

After propagating a certain distance into a turbulent medium the field becomes

$$U(t) = Ae^{i\omega t} e^{i\Phi} \tag{3.3}$$

where A and Φ represent the distorted amplitude and phase, respectively, induced by the medium.

It is customary to define the log-amplitude of the field by

$$\chi = \log(A/A_o) \tag{3.4}$$

so that $A = A_o e^{\chi}$. Hence, (3.3) can also be written

$$U(t) = A_o e^{\chi} e^{i(\omega t + \phi)}. \tag{3.5}$$

The intensity of the field is now given by

$$I = |U(t)|^2 = A_o^2 e^{2\chi} \tag{3.6}$$

and we define the log-intensity of the field by

$$\log(I/I_o) = 2\chi, \tag{3.7}$$

which equals twice the log-amplitude of the field.

For both plane-waves and spherical-waves the average intensity at a point can be taken as its value in the absence of turbulence, i.e.,

$$\langle I \rangle = I_o. \tag{3.8}$$

Under this assumption it follows from (3.6) that

$$\langle e^{2\chi} \rangle = 1. \tag{3.9}$$

The usual measure of the strength of the intensity fluctuations is the normalized variance defined by

$$\sigma^2 = \frac{\langle I^2 \rangle - \langle I \rangle^2}{\langle I \rangle^2} = \frac{\langle I^2 \rangle}{\langle I \rangle^2} - 1. \tag{3.10}$$

In terms of the log-amplitude χ, this reads

$$\sigma^2 = \langle e^{4\chi} \rangle - 1. \tag{3.11}$$

A. Probability Distribution of Log-Intensity:

Many theoretical investigations have concentrated on the random fluctuations in the log-intensity or log-irradiance. Under conditions of weak turbulence the log-intensity appears to satisfy a normal probability distribution, and hence the intensity itself is said to satisfy lognormal statistics. To theoretically see why this is so, we consider the following mathematical model.

Let us suppose the turbulent medium to be composed of a large number of independent slabs, oriented perpendicular to the direction of propagation of an optical beam, and such that the thickness of each slab is large compared with the outer scale of turbulence (see Fig. 3-1). Over short distances the scattering cone is narrow so most of the energy of the beam remains directed along the axis of propagation. Off-axis scattering terms are neglected.

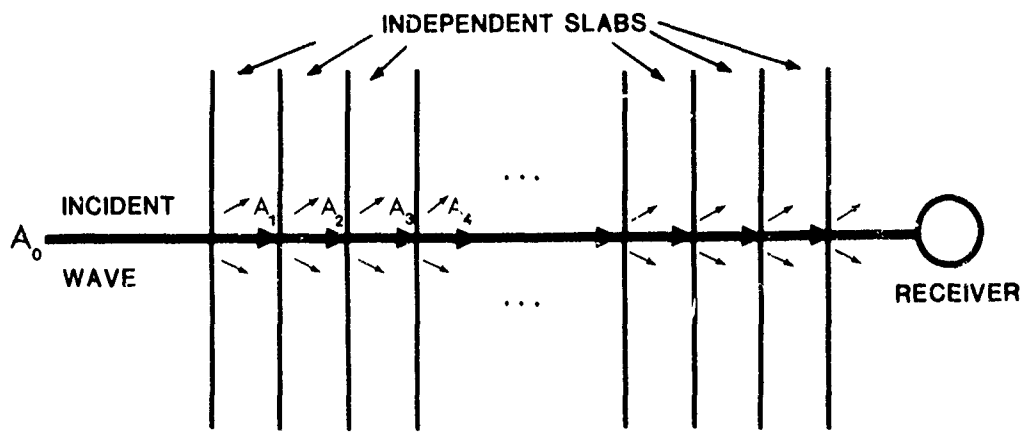

Fig. 1-1. Multiple scattering model with weak scattering within each layer.

The amplitude value of the wave is initially A_o. After passing through the first slab the amplitude is

$$A_1 = A_o - m_1 A_o = A_o(1 - m_1),$$

where m_1 is a "small" random proportionate. At the second slab the amplitude becomes

$$A_2 = A_1(1 - m_2) = A_o(1 - m_1)(1 - m_2)$$

whereas in general after n slabs, we have

$$A_n = A_o \prod_{j=1}^{n} (1 - m_j), \tag{3.12}$$

where the m_j's are assumed independent of each other. Taking the natural logarithm of (3.12) leads to

$$\text{Ln } A_n = \text{Ln } A_o + \sum_{j=1}^{\infty} \text{Ln}(1 - m_j), \tag{3.13}$$

and if n is sufficiently large ($n \to \infty$) we can invoke the Central Limit Theorem to declare that $\lim_{n\to\infty} \text{Ln } A_n = A$ is normally distributed.

Since we have defined

$$\chi = \text{Ln}(A/A_o) = \tfrac{1}{2} \text{Ln}(I/I_o), \tag{3.14}$$

it follows that χ is normally distributed with mean

$$\langle\chi\rangle = \tfrac{1}{2}\langle \mathrm{Ln}(I/I_o)\rangle \tag{3.15}$$

and variance

$$\sigma_\chi^2 = \langle\chi^2\rangle - \langle\chi\rangle^2. \tag{3.16}$$

The pdf for χ is therefore

$$p(\chi) = \frac{1}{\sqrt{2\pi}\,\sigma_\chi} \exp\{-(\chi - \langle\chi\rangle)^2/2\sigma_\chi^2\}, \tag{3.17}$$

and by putting $2\chi = \mathrm{Ln}(I/I_o)$, we get

$$p(I) = \frac{1}{2\sqrt{2\pi}\,\sigma_\chi I} \exp\{-[\mathrm{Ln}(I/I_o) - 2\langle\chi\rangle]^2/8\sigma_\chi^2\} \tag{3.18}$$

as the distribution for I. If we further introduce

$$\sigma_{\mathrm{Ln}I}^2 = \langle(\mathrm{Ln}(I/I_o))^2\rangle - \langle\mathrm{Ln}(I/I_o)\rangle^2,$$

called the log-intensity variance, we find

$$\sigma_{\mathrm{Ln}I}^2 = 4\langle\chi^2\rangle - 4\langle\chi\rangle^2 = 4\sigma_\chi^2. \tag{3.19}$$

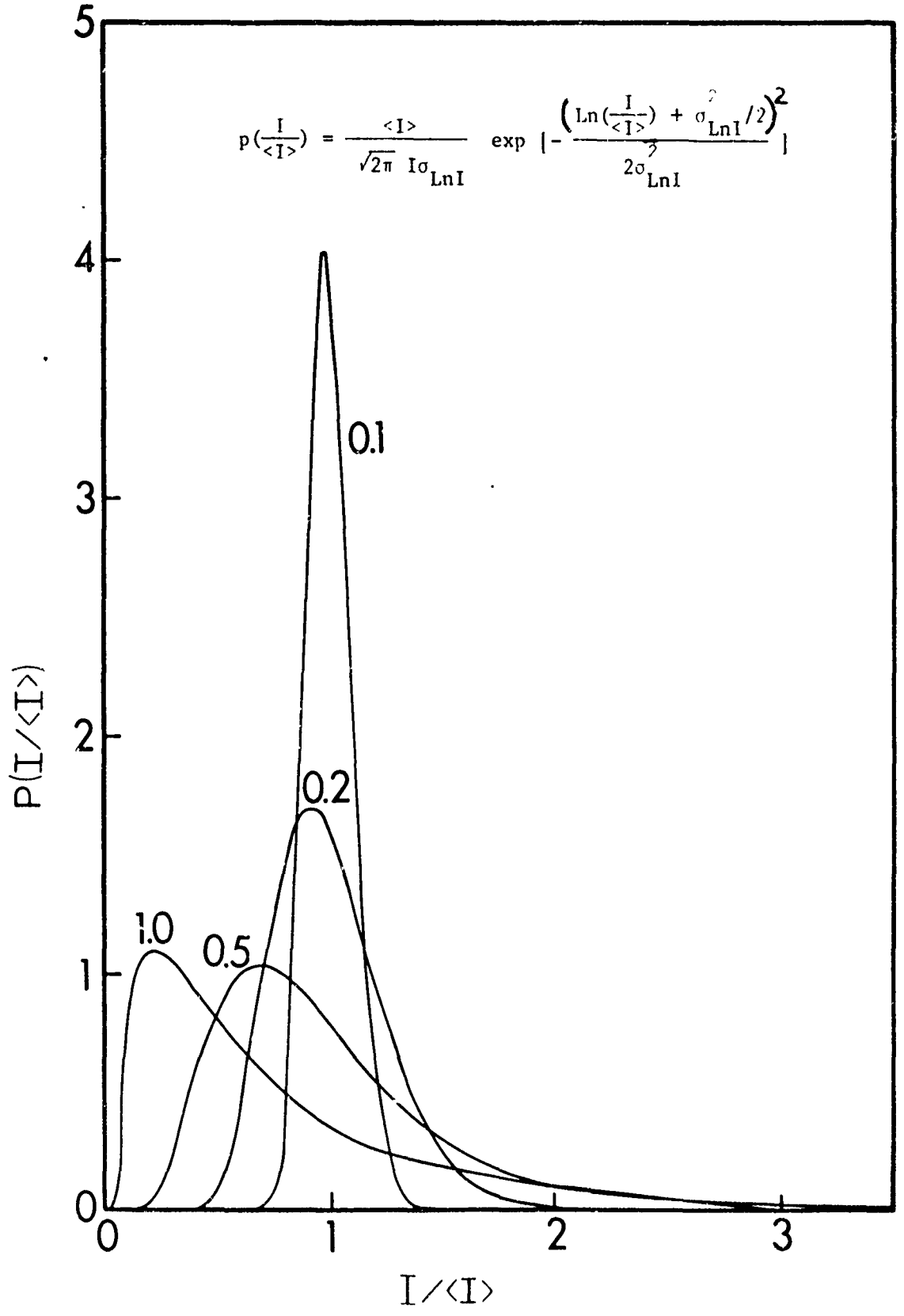

Fig. 3-2. Normalized lognormal distribution for various values of σ^2_{LnI}.

That is, the log-intensity variance is four times the log-amplitude variance, Using (3.19), we now write (3.18) in the more familiar form of the lognormal distribution,

$$p(I) = \frac{I^{-1}}{\sqrt{2\pi}\sigma_{LnI}} \exp\{-(\text{Ln } I - \nu)^2/2\sigma^2_{LnI}\}, \qquad (3.20)$$

where $\nu = \text{Ln } I_o + 2\langle\chi\rangle = \langle\text{Ln } I\rangle$ (see Fig. 3-2).

B. The Short Range Approximation:

If χ is normally distributed, then

$$\langle e^{2\chi}\rangle = \exp(2\langle\chi\rangle + 2\sigma^2_\chi)$$

and since $\langle e^{2\chi}\rangle = 1$ (Eq. (3.9)), it follows that $\langle\chi\rangle = -\sigma_\chi$. Therefore the normalized variance (3.11) leads to

$$\sigma^2 = \langle\exp(4\chi)\rangle - 1$$

$$= \exp(4\langle\chi\rangle + 8\sigma_\chi^2)$$

from which we deduce

$$\sigma^2 = \exp(4\sigma_\chi^2) - 1. \qquad (3.21)$$

In view of (3.19), we also note that

$$\sigma^2 = \exp(\sigma_{LnI}^2) - 1. \qquad (3.22)$$

The spherical wave theory [1], [5] predicts that the log-amplitude variance is proportional to the index of refraction structure parameter C_n^2 according to

$$\sigma_\chi^2 = 0.124\, C_n^2\, k^{7/6}\, L^{11/6}, \quad L \gg \ell_o^2/\lambda; \tag{3.23}$$

hence it follows that

$$\sigma_{LnI}^2 = 0.496\, C_n^2\, k^{7/6}\, L^{11/6}, \tag{3.24}$$

which is accepted valid for all ranges. However, if we restrict the log-intensity variance such that $\sigma_{LnI} \ll 1$, then

$$\exp(\sigma_{LnI}^2) \simeq 1 + \sigma_{LnI}^2$$

and thus (3.22) leads to the well-known approximation

$$\sigma^2 \cong \sigma_{LnI}^2 = 0.496\, C_n^2\, k^{7/6}\, L^{11/6}. \tag{3.25}$$

That is, under conditions of weak turbulence the variance of the intensity and the variance of the log-intensity are approximately equal. This same relation is no longer valid under conditions of strong turbulence where experimental evidence supports the point of view that σ^2 reaches a maximum value in the saturation regime and then decreases steadily toward a value of unity in the limit.

IV. EXPERIMENTAL MEASUREMENTS

Recently collected data tend to support once again the lognormal model for intensity fluctuations over short ranges or conditions of weak turbulence, whereas data recorded under conditions of strong turbulence (including distances up to 3000 meters) illustrate that the mean-square fluctuations $\langle I^2 \rangle / \langle I \rangle^2$ can be as high as 6. Neither the lognormal model nor the newly developed K-distribution [6], [9] are satisfactory for describing the observed phenomenon very well over all ranges of the mean-square fluctuations.

A. Experiment:

The propagation experiments which were conducted to verify the mathematical modelling were carried out at Kennedy Space Center's Space Shuttle Landing Facility. The Shuttle Landing Facility consists of a concrete runway 16,000 feet long (4.9 kilometers) and 300 feet wide. The area around the runway was cleared of all obstacles and vegetation for approximately a 1000 foot radius. The runway had weather monitoring stations at both ends and midway down the runway. Also, satellite weather pictures were received every 15 minutes of the Shuttle Landing Facility area along with the entire east central Florida area. This allowed the research team to plan and carry out the experiments under well documented conditions.

The experiments were conducted from March 17 to March 28, 1980. Tests were performed in the afternoon and at night. The daytime temperatures averaged 75 - 80° F while the nighttime temperatures averaged 66 - 68° F. The humidity remained low both during the daytime and nighttime experiments. The sky remained partially cloudy during the entire set of experiments but the winds varied considerably. During

the day, wind speeds ranged from 0 - 12 mph (0 - 5.36 m/s), while at night the wind was virtually still. Wind direction was usually parallel to the direction of propagation and less than half the time perpendicular to the propagation path.

The optical beam was generated by a Spectra Physics Model 120 HeNe laser with a wavelength of 632.8 nanometers and an inherent beam divergence of about 1 milliradian. The laser power was 15 milliwatts with an intensity fluctuation of less than 1% over a period of an hour. The optical beam was used directly from the laser without optics. A tripod was used to rigidly mount the laser transmitter at 1.4 meters above the runway surface. The runway was extremely flat which allowed the beam to remain at a constant height above the surface for ranges up to about 1000 meters. At ranges beyond 1000 meters the earth's natural curvature brought the beam to within ½ meter of the runway surface at some intermediate point of the path.

Two receiving stations were used to monitor the statistical fluctuation of the beam intensity. One station was located at a fixed distance of 183 meters from the transmitter while the second station was placed at several dfferent distances down range from both the transmitter and the first station. The short range station was used to measure the first and second statistical moments of the fluctuating laser beam. Extensive testing at this short range station confirmed that the statistics were indeed lognormal at this range.

The short range station consisted of a solid state PIN diode detector, a high gain transimpedance amplifier, filter (set at 2000 Hz), amplifier, and a special circuit designed to compute the normalized second moment of the fluctuating signal. The aperature of the detector

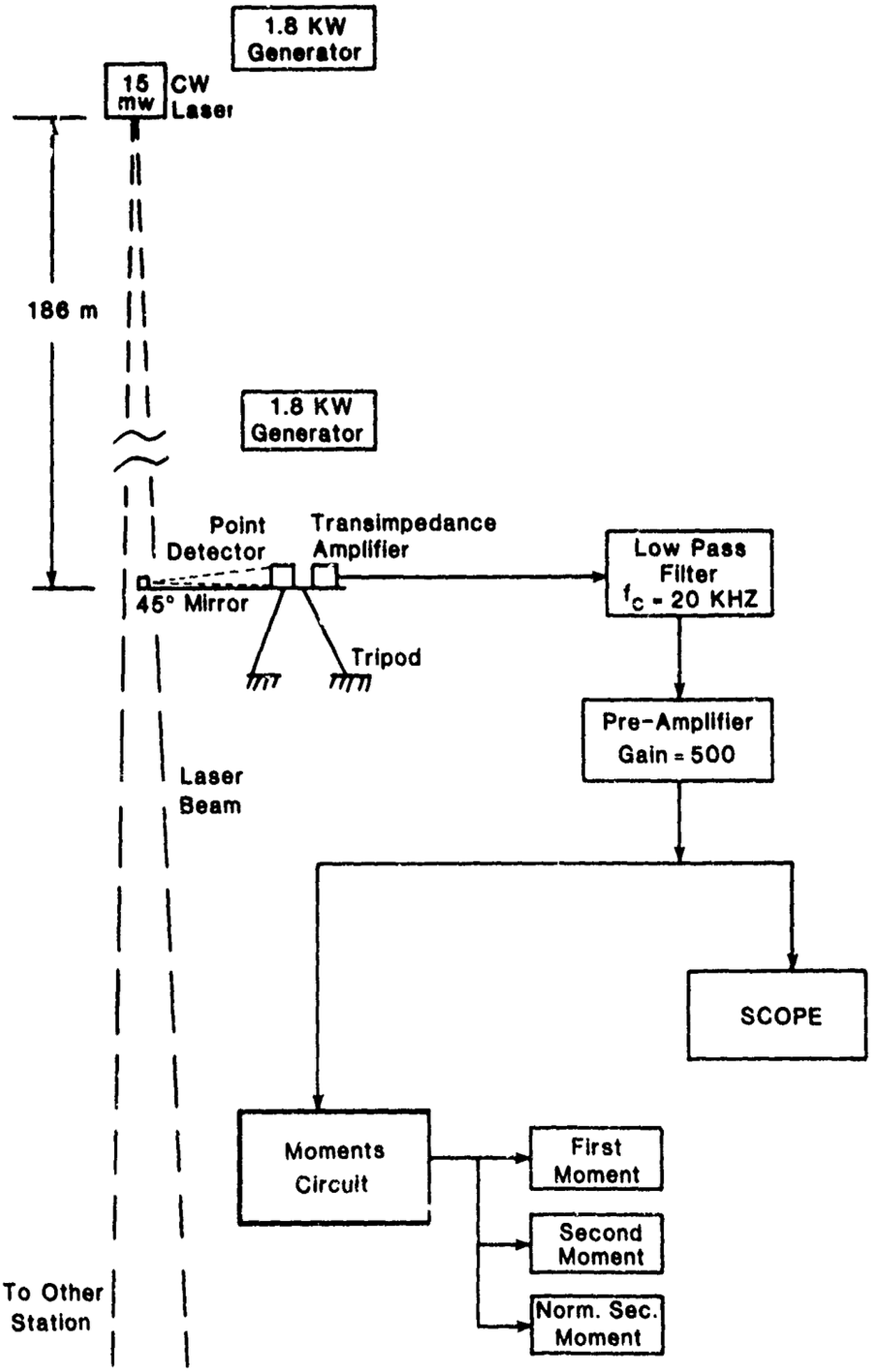

Fig. 4-1. System diagram of short range station.

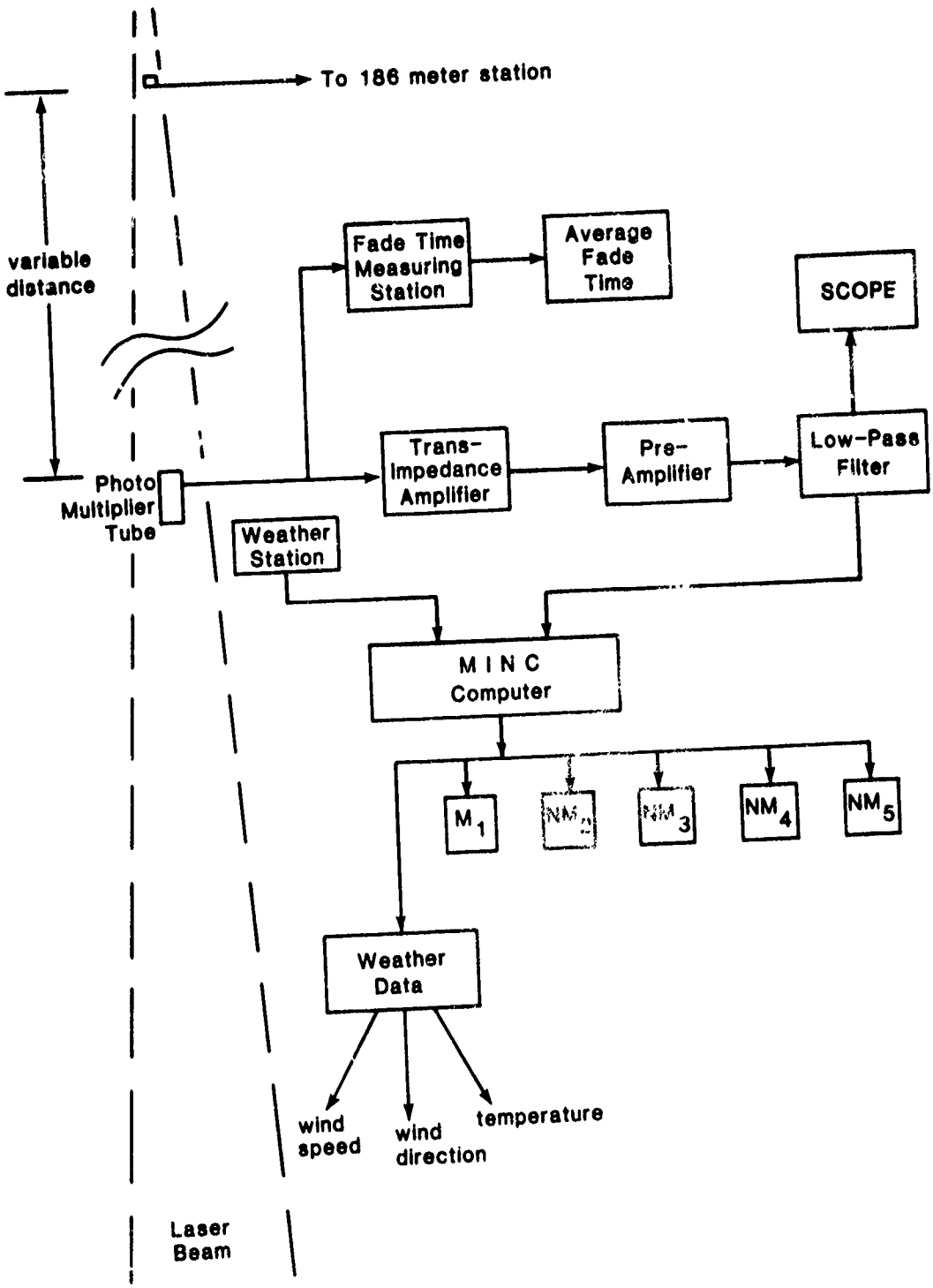

Fig. 4-2. System diagram of long range station.

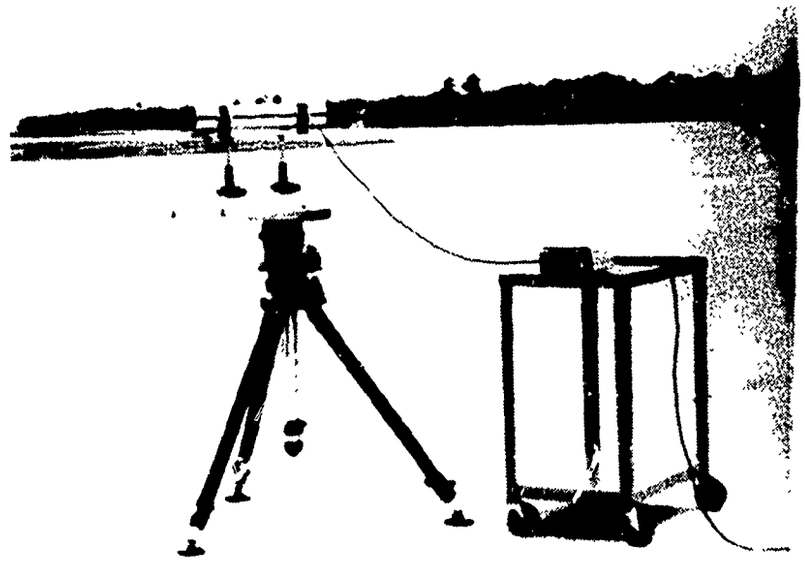

Fig. 4-3. Laser transmitter mounted on tripode 1.4 meters above runway surface.

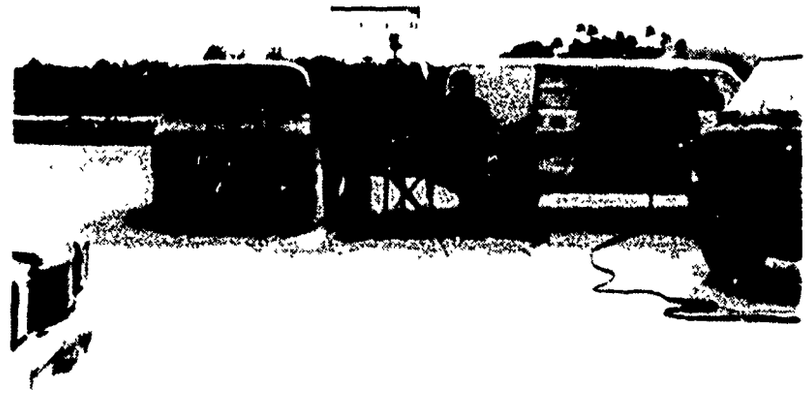

Fig. 4-4. Receiver at long range station.

Fig. 4-5. Looking towards laser transmitter from 1000 meters down range.

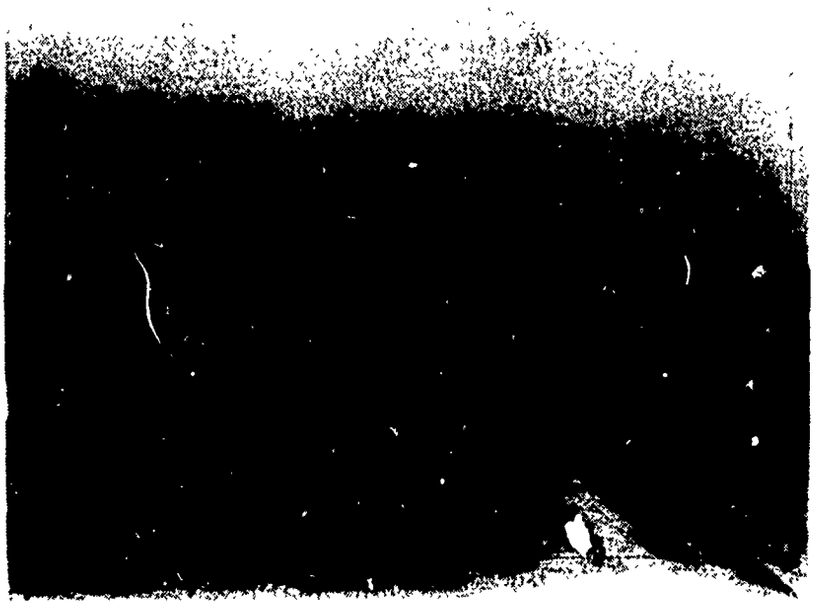

Fig. 4-6. Looking towards laser transmitter from 3000 meters down range.

Fig. 4-7. MINC-11 computer used to monitor the laser beam at long range station.

was ¼ millimeter and the detector was shielded from background light. Periodic checking of the background light and adjustment of the shield maintained a high signal-to-background ratio. A system diagram of the short range station is shown in Fig. 4-1.

At the long range station a photomultiplier detector was employed in conjunction with appropriate amplifiers and a Digital Equipment Corporation MINC-11 computer which digitized the signal and calculated the statistical moments (see Fig. 4-2). The aperature of the detector was set at 50μm so that the detector would function as a point detector. A high gain transimpedance amplifier followed the photomultiplier tube (PMT), the output of which was filtered to reduce the shot noise generated by the signal in the PMT. The signal was then amplified prior to the A/D converter. The A/D converter could accept signals bewteen +5 volts and -5 volts. The quantization level of the A/D converter was 2.5 millivolts. So as to obtain the lowest quantization noise level possible, the signal was kept at the highest possible level (without clipping). The sample rate by the computer of the analog signal was varied between 100 and 4000 samples per second. Occasionally the background light was checked by turning off the laser and then having the computer sample the background light alone. The photographs in Figures 4-3 through 4-7 show the actual experimental equipment used during the test.

B. Results:

The analysis of the fluctuating optical signal was performed by computing the first five statistical moments of the measured signal. The computer was programmed to calculate and display the moments as data was being taken. Normalized moments were calculated by dividing the nth moment $\langle I^n \rangle$ by the average value $\langle I \rangle$ raised to the nth power,

i.e., $\langle I^n \rangle / \langle I \rangle^n$. This normalization process allows one to discern the inherent statistics of the scattering process independent of the power of the laser beam and allows for a comparison of the statistics at different ranges. The moments give information about the shape of the probability density function. Comparisons of the cumulative probability curves can be deceiving in that different cumulative curves may appear to be very similar but yet the distributions from which they came may differ greatly out in the "wings" of the distribution. It is these "wings" that are of most importance in long range propagation, and since the moments high-light the differences between the "wings" of various distributions, we have chosen them as a means of discriminating between distributions rather than relying on cumulative probability curves.

Fig. 4-8 shows a plot of the measured normalized moments $\langle I^n \rangle / \langle I \rangle^n$ for n = 3,4,5 as a function of the normalized second moment $\langle I^2 \rangle / \langle I \rangle^2$. It is interesting to note that the normalized second moment takes on values as high as 5 and 6. However, these high values seem to be consistent with other recently measured data [9]. For a fixed value of $\langle I^2 \rangle / \langle I \rangle^2$ the data in the figure gives the appearance of being widely scattered. Actually this is due to the fact that the moments steadily increase until they reach a maximum value and then begin to slowly decrease. As they decrease the moments assume values lower than corresponding values attained during the time of increase for a fixed value of $\langle I^2 \rangle / \langle I \rangle^2$.

Fig. 4-8 also shows graphs of the lognormal and K-distributions having the same first and second moments as the data. For small values of $\langle I^2 \rangle / \langle I \rangle^2$ the data does indeed substantiate the lognormal model and

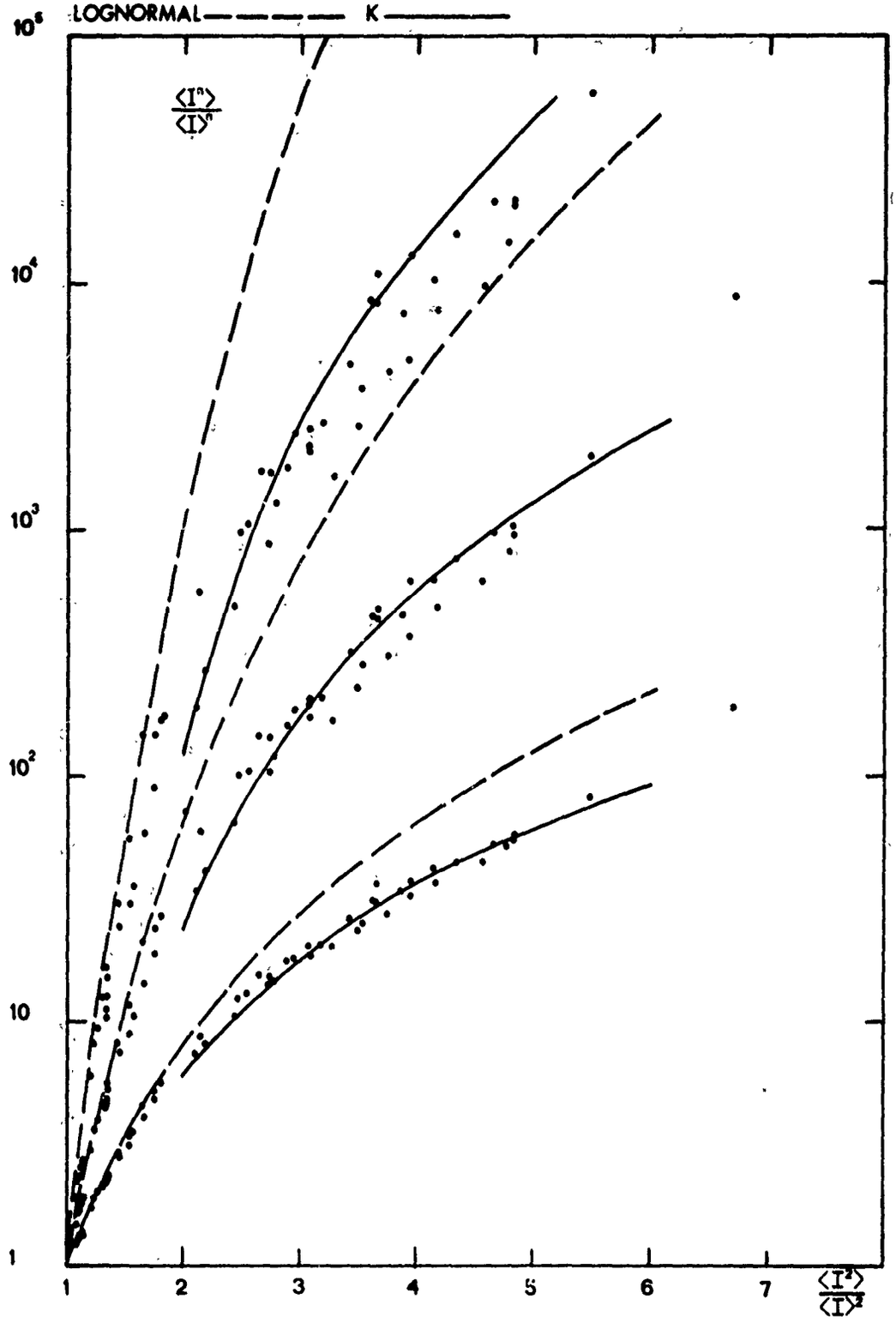

Fig. 4-8. Measured values of the normalized third, fourth and fifth moments as compared with values expected from the lognormal and K-distributions. The dashed line is associated with the lognormal model and the continuous line with the K-distribution.

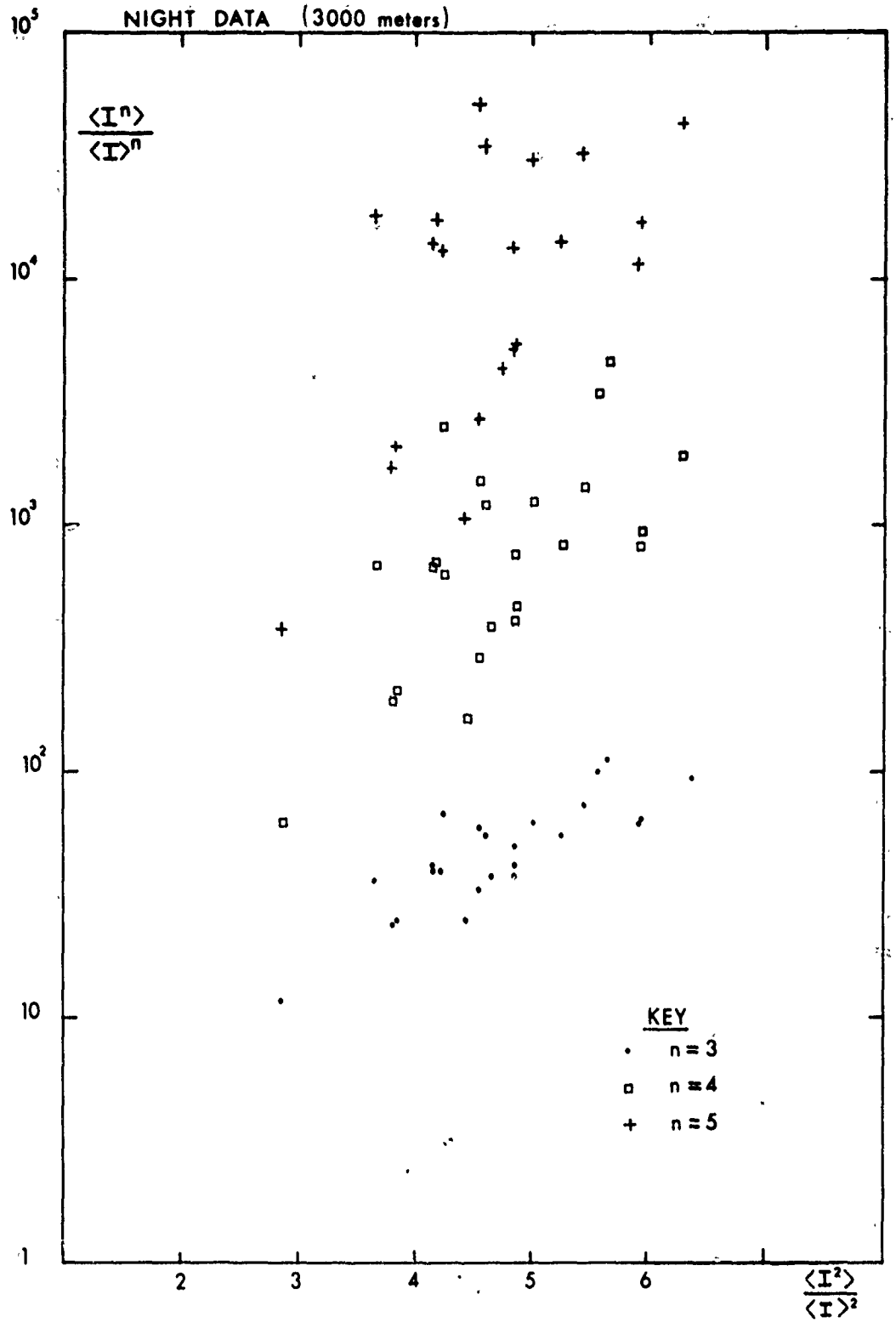

Fig. 4-9. Nighttime data with zero wind velocity.

the K-distribution appears to fit the data reasonably well for larger values of the normalized second moment. However, neither distribution provides the looping effect previously mentioned where the moments reach a maximum value and then decrease along different curves.

Data gathered during the nighttime hours at a distance of 3000 meters is shown in Fig. 4-9. The wind velocity was virtually zero. The wide scattering of the data is attributed to the fact that the weather conditions led to a state of nonstationary statistics.

V. A NEW THEORETICAL MODEL FOR INTENSITY FLUCTUATIONS

Limitations of the lognormal model for describing random intensity fluctuations have been widely recognized in the literature. Even the newly developed K-distribution is limited to only certain conditions of turbulence. Therefore it seems highly desirable to develop a universal model which has characteristics of the lognormal model under conditions of weak turbulence ($\sigma^2_{LnI} << 1$) and characteristics of the K-distribution for conditions of strong turbulence ($\sigma^2_{LnI} >> 1$).

The lognormal model emerged under the hypothesis that virtually all of the energy of the optical beam is directed along the axis of propagation and ignores the multiple scattering effects of the off-axis eddies. Under conditions of strong turbulence the contributions from the off-axis are more significant than the line-of sight contribution so that ignoring these scattering effects can no longer be valid.

Following along similar lines as in deWolf's [4] physical model, we believe it is reasonable to argue about the existence of two principal components which contribute to the field received at a point downrange from the transmitter. One of these components, called the specular component, results from the forward scattering by the large eddies along the propagation axis as described in the lognormal model in Section III-A. The second component which we refer to as the diffuse component(s) arrives at the point receiver after multiple scattering by the off-axis eddies (see Fig. 5-1). Thus the received field is described mathematically by

$$U(t) = \underbrace{(Ae^{i\theta}}_{\text{specular component}} + \underbrace{Re^{i\phi})}_{\text{diffuse component}} e^{i\omega t}. \qquad (5.1)$$

Similar models have previously been suggested also by Jao and Elbaum [8] and Fante [15].

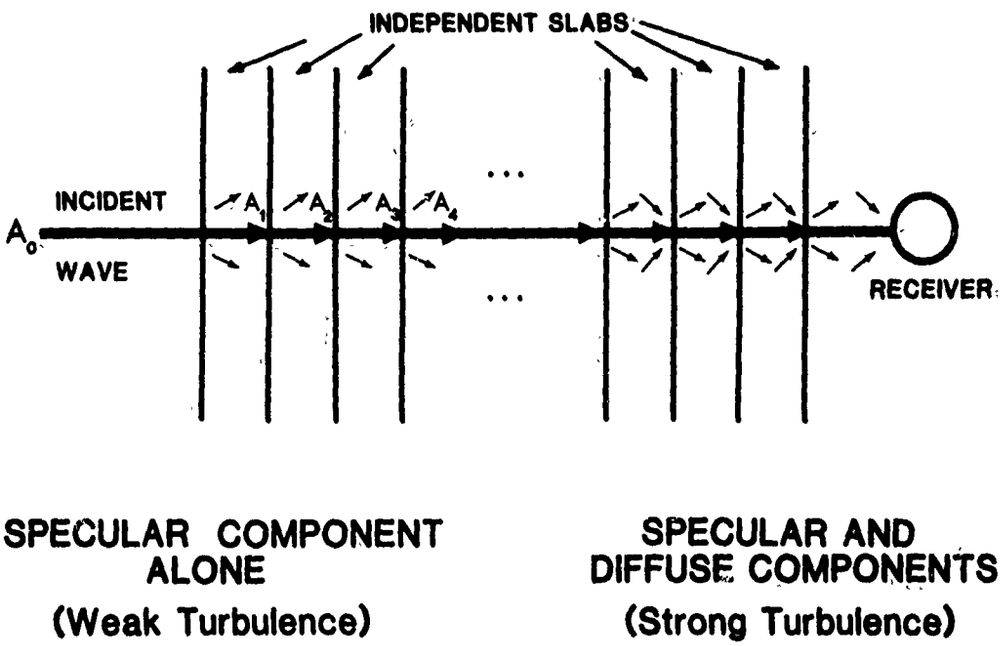

Fig. 5-1. Multiple scattering model.

Based upon physical considerations it can be argued that the amplitude A of the specular component essentially satisfies the log-normal probability distribution and that the phase angle θ is uniformly distributed. These assumptions are consistent with deWolf's model. However, deWolf assumes that the amplitude R of the diffuse component(s)

obeys a Rayleigh distribution. Surely this must be the case in the limit where essentially all of the energy of the beam is contained within the diffuse component(s) and the number of terms contributing to this component is large. In intermediate regimes we believe the diffuse component is the result of adding a small number of terms so that the Rayleigh assumption is not justified. Therefore we choose to make the assumption that R satisfies a generalized Rayleigh distribution which includes the Rayleigh distribution, among others, as a special case. As for the specular component, the phase angle ϕ is assumed uniformly distributed.

The generalized Rayleigh distribution, also called the m-distribution, was first introduced by Nakagami [16] in connection with his studies of intensity distributions for rapid fading in long distance propagation. Much of his work was done during the 1940's and published in Japanese journals which may account for the fact that some of his work has gone on virtually unnoticed. The m-distribution seems appropriate here also in connection with our problem because of the close smilarities of the phenomena and because it leads to the Rayleigh distribution as a limiting case.

A. Development of the PDF:

Assuming the received field within a region of turbulence is given by (5.1), the intensity of the field is found to be

$$I = |U(t)|^2 = A^2 + R^2 + 2AR\cos(\phi - \theta). \qquad (5.2)$$

Although there are several approaches that could be used for calculating the pdf for I, we do so by utilizing the Hankel transform (see Appendix A)

$$p(I) = \tfrac{1}{2} \int_0^\infty zC(z)J_0(\sqrt{I}\, z)dz \tag{5.3}$$

where

$$C(z) = \int_0^\infty p(A)J_0(Az)dA \int_0^\infty p(R)J_0(Rz)dR \tag{5.4}$$

is a characteristic function. The function $J_0(.)$ is the Bessel function of the first kind of order zero ([17], pp. 355-434) and p(A) and p(R) denote the pdfs associated with the amplitudes A and R, respectively.

Under the assumption that R satisfies the m-distribution, we have [16] (see Fig. 5-2).

$$p(R) = \frac{2m^m R^{2m-1}}{\Gamma(m)\, b^m} e^{-mR^2/b}, \tag{5.5}$$

where $b = \langle R^2 \rangle$ is the average of the intensity R^2 and $\Gamma(.)$ is the gamma function (see [17], pp. 253-294). Observe that for m = 1, (5.5) reduces to the well-known Rayleigh distribution. Thus we find

$$\int_0^\infty p(R)J_0(Rz)dR = \frac{2\, m^m}{\Gamma(m)b^m} \int_0^\infty R^{2m-1}\, e^{-mR^2/b}\, J_0(Rz)dR$$

$$= {}_1F_1(m;1;-bz^2/4m), \tag{5.6}$$

where we have used the formula ([18], p. 716)

$$\int_0^\infty x^\mu e^{-\alpha x^2} J_\nu(\beta x)dx = \frac{\Gamma\left(\frac{\nu+\mu+1}{2}\right)\beta^\nu}{2^{\nu+1}\,\alpha^{(\nu+\mu+1)/2}\,\Gamma(\nu+1)} {}_1F_1\left(\frac{\nu+\mu+1}{2};\nu+1;-\frac{\beta^2}{4\alpha}\right) \tag{5.7}$$

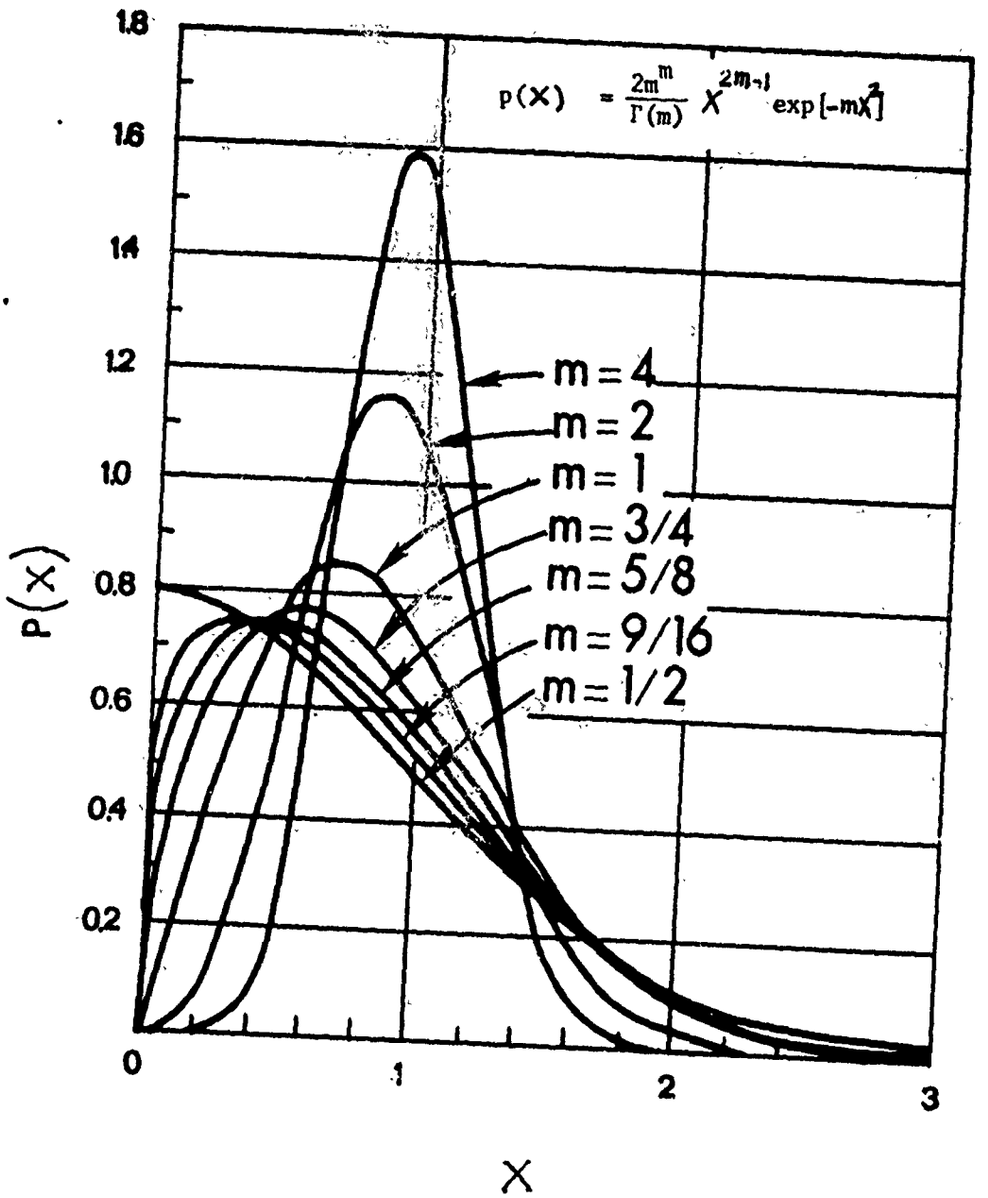

Fig. 5-2. The normalized m-distribution.

Here ${}_1F_1(a;b;c)$ is the confluent hypergeometric function ([17], pp. 503-536). If A is assumed to be lognormal, the first integral in (5.4) cannot be evaluated in closed form. We therefore resort to the power series expansion

$$J_o(x) = \sum_{k=0}^{\infty} \frac{(-1)^k (x/2)^{2k}}{(k!)^2} \tag{5.8}$$

so that

$$\int_o^{\infty} p(A) J_o(Az)\,dz = \sum_{k=0}^{\infty} \frac{(-1)^k (z/2)^{2k}}{(k!)^2} \int_o^{\infty} A^{2k}\, p(A)\,dA$$

$$= \sum_{k=0}^{\infty} \frac{(-1)^k (z/2)^{2k} \langle A^{2k} \rangle}{(k!)^2}\,, \tag{5.9}$$

where $\langle A^{2k} \rangle$ denotes the kth moment of A^2. Now (5.3) becomes

$$p(I) = \tfrac{1}{2} \sum_{k=0}^{\infty} \frac{(-1)^k \langle A^{2k} \rangle}{2^{2k} (k!)^2} \int_o^{\infty} z^{2k+1}\, {}_1F_1(m;1;-bz^2/4m) J_o(\sqrt{I}\, z)\,dz, \tag{5.10}$$

or owing to the integral formula ([18], p. 873)

$$\int_o^{\infty} x^{2\rho}\, {}_1F_1(a;b;-\lambda x^2) J_\nu(xy)\,dz = \frac{2^{2\rho}\,\Gamma(b)}{\Gamma(a)\, y^{2\rho+1}} G_{23}^{21}\left(\frac{y^2}{4\lambda} \,\middle|\, \begin{matrix} 1, & b \\ \frac{\nu+1}{2} + \rho, & a, \quad \frac{1-\nu}{2} + \rho \end{matrix} \right), \tag{5.11}$$

(5.10) reduces to

$$p(I) = \sum_{k=0}^{\infty} \frac{(-1)^k \langle A^{2k} \rangle}{(k!)^2\, \Gamma(m)}\, I^{-(k+1)}\, G_{23}^{21}\left(\frac{mI}{b} \,\middle|\, \begin{matrix} 1, & 1 \\ k+1, & m, \quad k+1 \end{matrix} \right), \tag{5.12}$$

which we shall henceforth refer to as the G-distribution or universal model. The function $G_{pq}^{mn}(.)$ is a generalized function known as the Meijer G-function ([19], p. 206).

Although (5.12) is a representation for the pdf associated with intensity fluctuations, it does not lend itself in its present form to easy computations because of the complexity of the G-function. In Appendix B we relate this particular G-function to the associated Laguerre functions, but even so the resulting expression is still quite complex. Further refinement of this pdf is called for in order to make it more tractable.

B. Theoretical Moments:

For purposes of comparing a probabilistic theoretical model with experimental data we believe a comparison of the predicted (normalized) moments with the actual (normalized) moments provides a better criterion for validating the model than does a comparison of the distributions themselves or their cumulative probabilities. With few exceptions, the moments uniquely determine the distribution.

While the pdf (5.12) does not readily lend itself to direct computations for the pdf or the cumulative probability, it does lead to a closed form expression for the moments. Thus if we use the integral formula ([18], p. 897)

$$\int_0^\infty x^{\rho-1} G_{pq}^{mn}\left(\alpha x \middle| \begin{matrix} a_1,\ldots,a_p \\ b_1,\ldots,b_q \end{matrix}\right) dx = \frac{\prod_{j=1}^{m} \Gamma(b_j+\rho) \prod_{j=1}^{n} \Gamma(1-a_j-\rho)}{\prod_{j=m+1}^{q} \Gamma(1-b_j-\rho) \prod_{j=n+1}^{p} \Gamma(a_j+\rho)} \alpha^{-\rho}, \quad (5.13)$$

we find

$$\langle I^n \rangle = \int_0^\infty I^n \, p(I) dI$$

$$= \sum_{k=0}^{\infty} \frac{(-1)^k \langle A^{2k} \rangle}{(k!)^2 \, \Gamma(m)} \int_0^\infty I^{n-k-1} \, G_{23}^{21} \left(\frac{mI}{b} \middle|_{k+1,\, m,\, k+1}^{1,\, 1} \right) dI$$

$$= \sum_{k=0}^{n} \frac{(-1)^k \langle A^{2k} \rangle}{(k!)^2 \, \Gamma(m)} \left(\frac{b}{m} \right)^{n-k} \frac{n! \, \Gamma(m + n - k) \, \Gamma(k - n)}{(n - k)! \, \Gamma(-n)} , \qquad (5.14)$$

where the series is now finite. That is, all terms such that $k \geq n + 1$ reduce to zero because of the factorial $(n - k)!$ in the denominator. Also,

$$\frac{\Gamma(k - n)}{\Gamma(-n)} = (-1)^k \, n(n-1)\ldots(n - k + 1) = \frac{(-1)^k \, n!}{(n - k)!}$$

and thus (5.14) is equivalent to

$$\langle I^n \rangle = \sum_{k=0}^{n} \binom{n}{k}^2 \frac{b^{n-k} \Gamma(m + n - k) \langle A^{2k} \rangle}{m^{n-k} \, \Gamma(m)} , \qquad (5.15)$$

where

$$\binom{n}{k} = \frac{n!}{k!(n - k)!} .$$

In order to make comparisons of the moments of various distributions they should be normalized so that the mean value is unity. To do so, we first set $n = 1$ in (5.15) to get

$$\langle I \rangle = b + \langle A^2 \rangle = b(1 + r) \qquad (5.16)$$

where $r = \langle A^2 \rangle / b = \langle A^2 \rangle / \langle R^2 \rangle$ is the power ratio of mean intensities of the specular to diffuse components. It is also convenient to introduce the normalized moments [16], [20]

$$\mu_k = \frac{\langle R^{2k} \rangle}{\langle R^2 \rangle^k} = \frac{\Gamma(m + k)}{m^k \, \Gamma(m)} \tag{5.17}$$

and

$$a_k = \frac{\langle A^{2k} \rangle}{\langle A^2 \rangle^k} = \lambda^{k(k-1)/2}, \tag{5.18}$$

where $\lambda = \langle A^4 \rangle / \langle A^2 \rangle^2$. Hence we now write

$$\langle I^n \rangle = b^n \sum_{k=0}^{n} \binom{n}{k}^2 \mu_{n-k} \, a_k \, r^k$$

so upon division by $\langle I \rangle^n$, we finally obtain

$$\frac{\langle I^n \rangle}{\langle I \rangle^n} = \frac{1}{(1 + r)^n} \sum_{k=0}^{n} \binom{n}{k}^2 \mu_{n-k} \, a_k \, r^k. \tag{5.19}$$

It might be of interest to note here that limiting forms of (5.19) lead to normalized moments of either the lognormal distribution ($r \to \infty$) or the negative exponential distribution ($r \to 0$), i.e.,

$$\frac{\langle I^n \rangle}{\langle I \rangle^n} = \begin{cases} \lambda^{n(n-1)/2} & \text{as } r \to \infty \\ n! & \text{as } r \to 0, \end{cases}$$

in agreement with previous theories. (As $r \to 0$, we also have $m \to 1$ in (5.17) to get this result.)

C. Comparison of Moments with Data:

The normalized moments (5.19) depend upon three parameters:

(a). the reciprocal of the normalized variance of the m-distribution denoted by m,

(b). the normalized second moment λ of the lognormal distribution, and

(c). the power ratio r of mean intensities of the specular to diffuse components.

The three parameters m, λ, r are chosen in such a way that the first two normalized moments of I match the data identically and the third moment is matched by some "best fit" criterion.

Since only the first five normalized moments were actually measured in the field, we separately list the corresponding theoretical moments as determined by (5.19),

$$\frac{\langle I \rangle}{\langle I \rangle} = 1, \tag{5.20a}$$

$$\frac{\langle I^2 \rangle}{\langle I \rangle^2} = \frac{\mu_2 + 4r + a_2 r^2}{(1 + r)^2}, \tag{5.20b}$$

$$\frac{\langle I^3 \rangle}{\langle I \rangle^3} = \frac{\mu_3 + 9\mu_2 r + 9a_2 r^2 + a_3 r^3}{(1 + r)^3}, \tag{5.20c}$$

$$\frac{\langle I^4\rangle}{\langle I\rangle^4} = \frac{\mu_4 + 16\mu_3 r + 36\mu_2 a_2 r^2 + 16 a_3 r^3 + a_4 r^4}{(1+r)^4}, \tag{5.20d}$$

$$\frac{\langle I^5\rangle}{\langle I\rangle^5} = \frac{\mu_5 + 25\mu_4 r + 100\mu_3 a_2 r^2 + 100\mu_2 a_3 r^3 + 25 a_4 r^4 + a_5 r^5}{(1+r)^5}. \tag{5.20e}$$

Here we note that $\mu_1 = a_1 = 1$,

$$a_k = \lambda^{k(k-1)/2}, \quad k = 2,3,4,5$$

and

$$\mu_{k+1} = (1 + k/m)\mu_k, \quad k = 1,2,3,4,$$

this last result being derived from (5.17).

The measured normalized moments $\langle I^n\rangle/\langle I\rangle^n$ for $n = 3,4,5$ as a function of the normalized second moment $\langle I^2\rangle/\langle I\rangle^2$ are shown in Fig. 5-3 along with theoretical curves predicted by the present G-distribution (Eq. (5.20a) - (5.20e)). In Fig. 4-8 the same data was displayed along with theoretical curves predicted by the lognormal distribution and K-distribution.

Although the moments as given by Eq. (5.19) depend upon three parameters, we found that a reduction to one effective parameter could be realized by utilizing empirical relations such as

$$\lambda \approx 0.59x + 0.41 \tag{5.21}$$

and

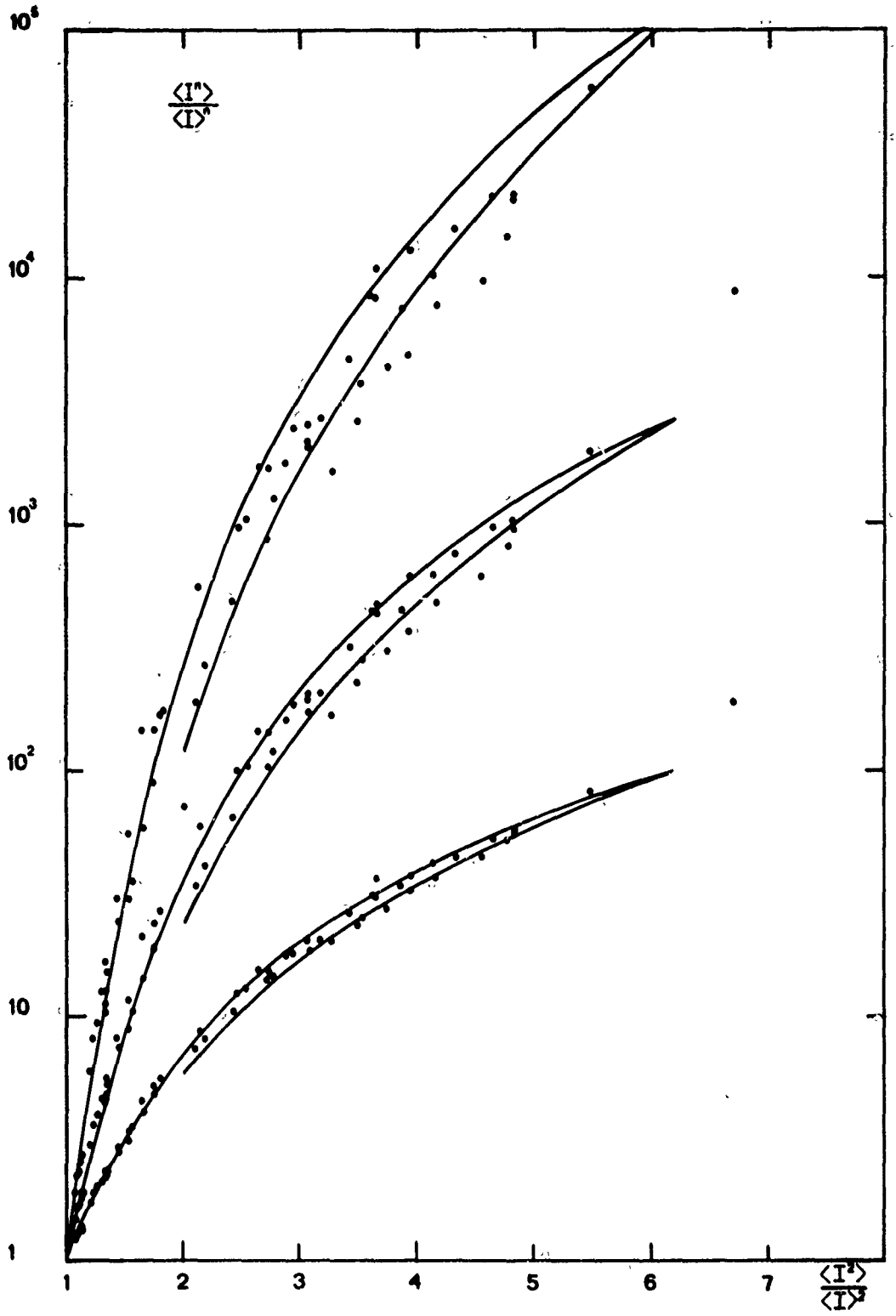

Fig. 5-3. Measured values of the normalized third, fourth and fifth moments as compared with values expected from the G-distribution or universal model.

$$\mu_2 = \begin{cases} -0.396x^2 + 5.902x - 4.506, & \sigma_{LnI} < 2 \\ 0.2375x^2 + 1.4625x - 1.875, & \sigma_{LnI} > 2 \end{cases} \tag{5.22}$$

where $x = \langle I^2 \rangle / \langle I \rangle^2$. That is, we found the normalized second moment associated with the specular component varying almost linearly with the total intensity second moment whereas a relationship involving the normalized second moment associated with the diffuse component required a quadratic relation which further depended upon the value of the log-intensity variance. The parameter m is then calculated from (5.22) and the relation

$$m = 1/(\mu_2 - 1). \tag{5.23}$$

The one remaining parameter r can therefore be expressed as a function of λ, μ_2 and x by utilizing (5.20b) from which we deduce the relation

$$r = \frac{2 - x + \sqrt{(\mu_2 + \lambda - 4)x + 4 - \lambda\mu_2}}{x - \lambda} . \tag{5.24}$$

Using the empirical relations (5.21) and (5.22) along with (5.23) and (5.24), the variation of the intensity σ^2 and the variation of the power ratio r as functions of σ_{LnI} or σ^2_{LnI} are shown in Fig.'s 5-4 and 5-5, respectively.

We should hasten to point out that the empirical relations (5.21) and (5.22) were not arrived at by applying some regression relation in the hopes of finding the best fit. Since the actual amount of data available at this time is somewhat sparse, we employed visual fits

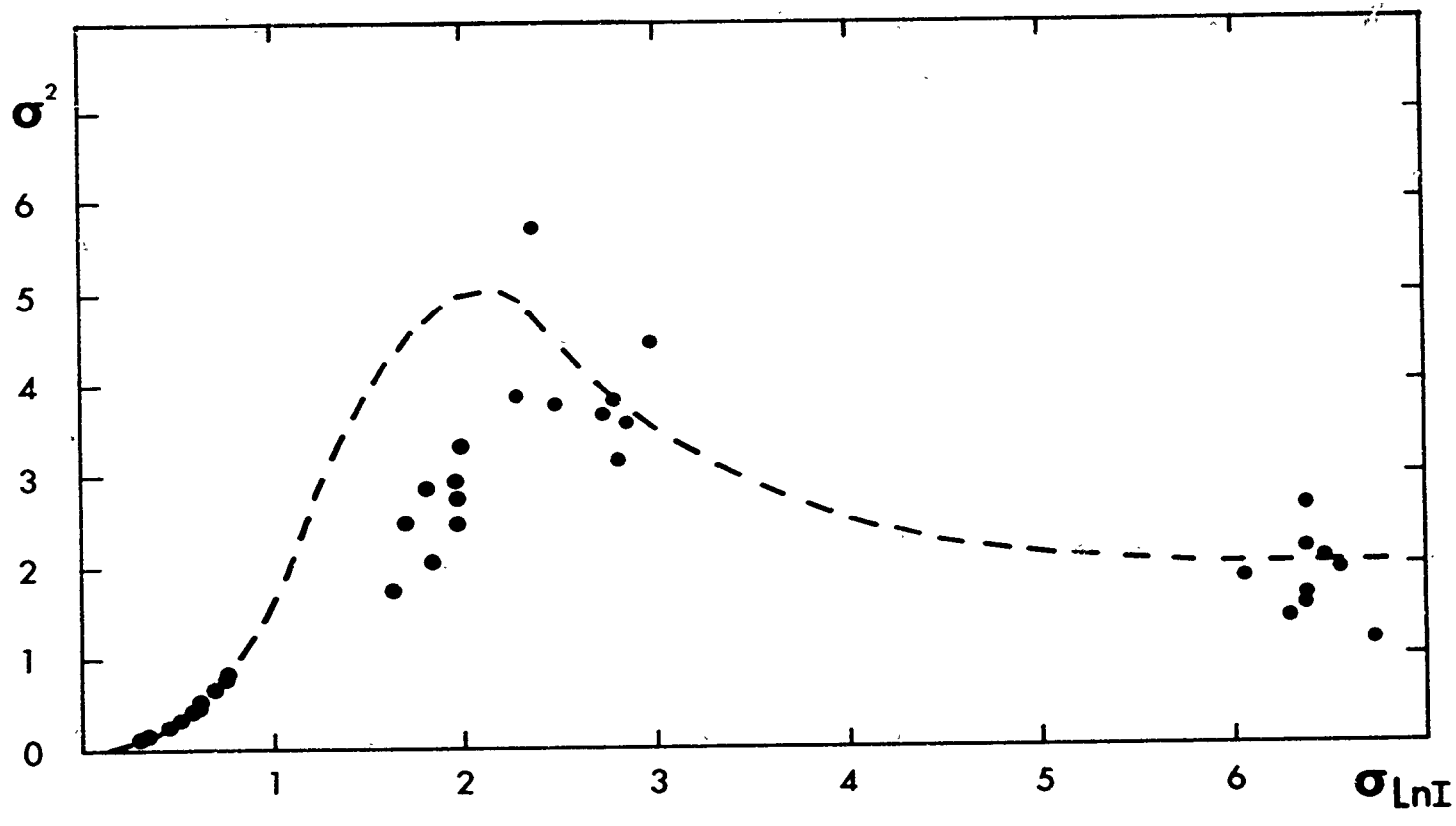

Fig. 5-4. Measured normalized variance versus predicted σ_{LnI}. The dashed curve represents theoretical model.

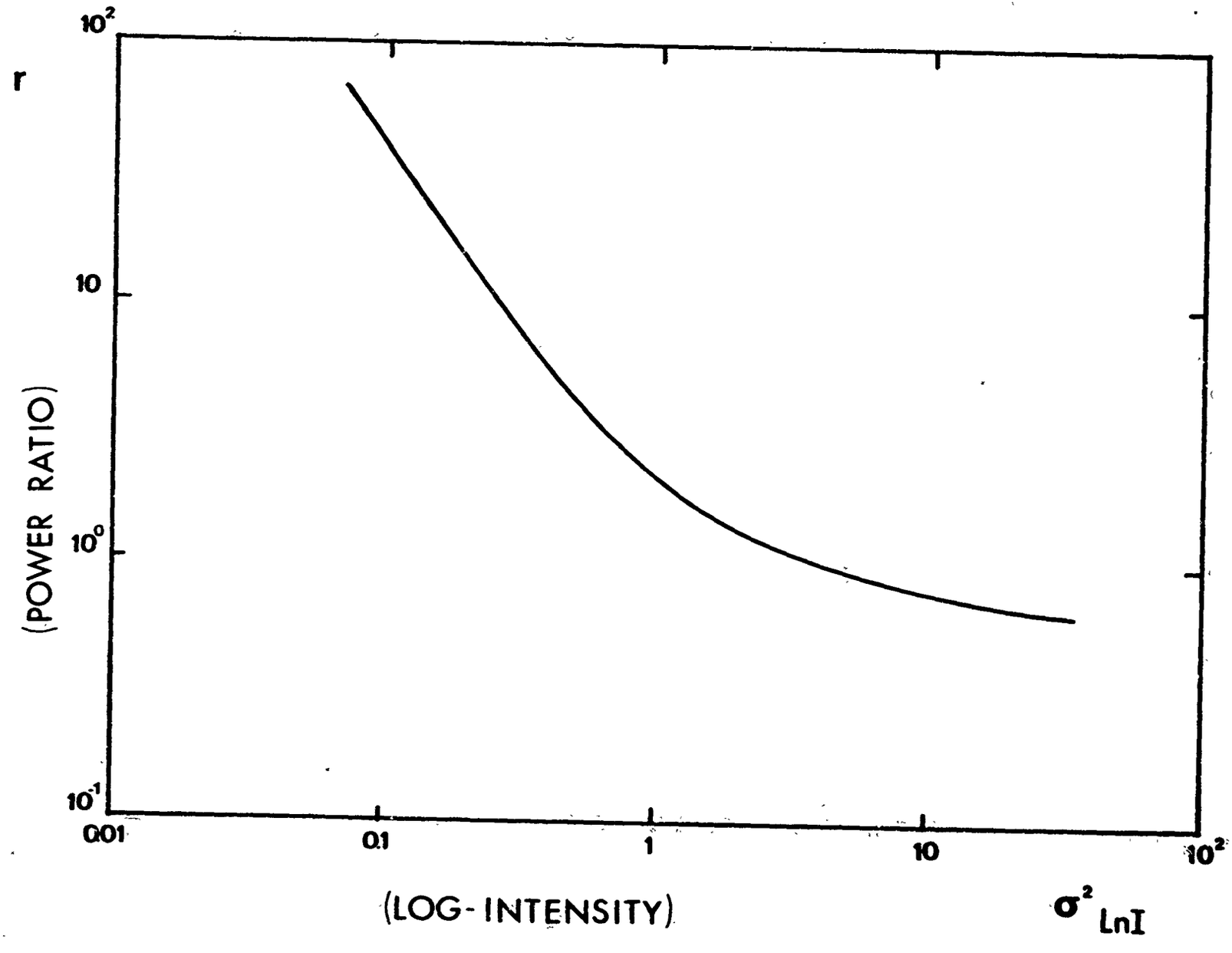

Fig. 5-5. The power ratio of mean intensity of specular to diffuse components of scattered laser beam.

based upon the data that we obtained as well as using data that was earlier published by Parry and Pusey [9]. It is likely that some modification of these relations will result when more data is available so that a better fit of the theoretical curves can be obtained.

VI. BINARY UNION DECODING

The Binary Union Decoder is a decoding technique used to recognize block codes which are transmitted through a fading channel. The MILES system uses such a decoder in order to defeat the fading of a laser beam signal caused by scintillation (or other scattering mechanisms).

The decoder consists of one storage register that acts like a memory for a word. The next received word is then OR'ed bit by bit with the word that preceded it and which was stored in the memory register. The result is a word which is then decoded. This technique is designed to make up for the loss of one half of a word so long as the same half of the word is not lost in each word transmission.

A conceptual block diagram of the decoder is shown in Fig. 6-1, illustrating that each of the bits in the stored word is OR'ed with its corresponding bit in the current incoming word. The fact that each bit is used twice, once when it enters the receiver and once after it has subsequently been stored in memory, means that the OR'ed words shown schematically in the right-hand column are not independent of one another. It is precisely this dependence between the OR'ed words that was ignored in an earlier analysis of the decoder and thereby lead to an overly-optimistic prediction of the MILES System performance [21].

In this section of the report we present a detailed analysis of the Binary Union Decoder taking into account the dependence between OR'ed words. We consider MILES block code words with weight W and N+1 repeated word transmissions. Special cases to be considered are the following:

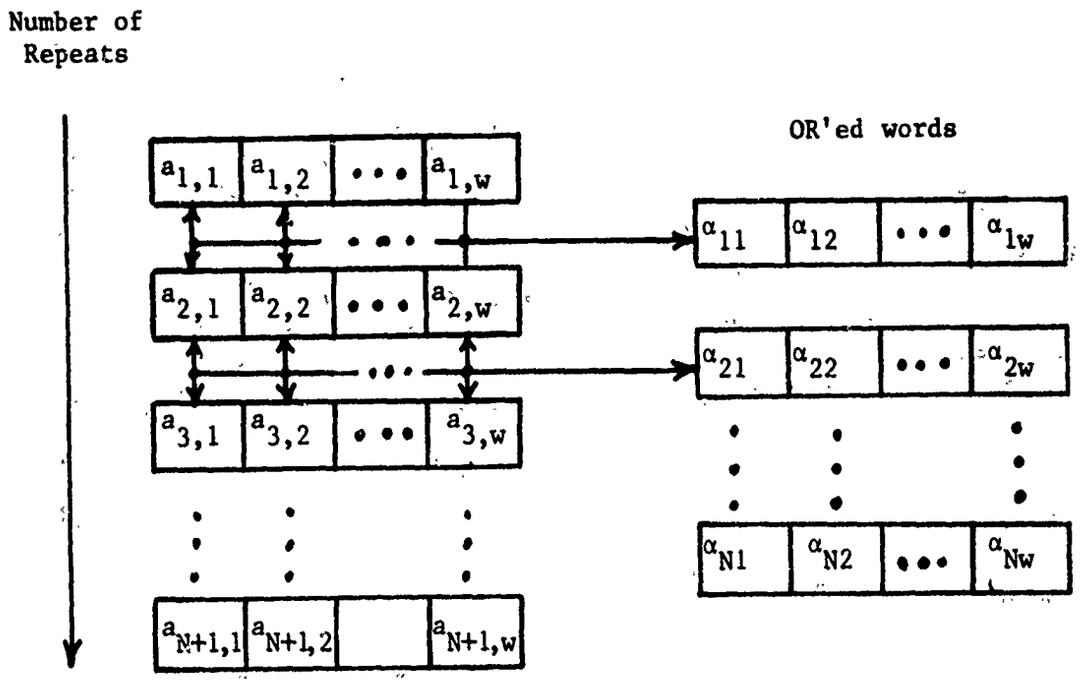

Fig. 6-1. Block diagram of Binary Decoder.

Case I: All bits in each word have equal probability p and the word detection probability computed for N = 4 and N = 8. (This case simulates the situation wherein the statistics of the propagation path of the laser beam remains constant during the entire message transmission.) These results are compared with the current MILES analysis [21] where independence between OR'ed words was assumed.

Case II: All bits in the first half of each word have equal probability p and all bits in the second half of the word have equal probability q, where $q = 3p/4$. (This case models the fading of half a word length, and since the MILES word is 3.63 milliseconds in duration, it corresponds to the case of 1.8 milliseconds average fade time.)

Case III: All bits in the first half of each word have equal probability, and this probability is the same as associated with all bits in the last half of the preceding word. Thus half the word has probability p and the other half has probability $q = 3p/4$. (This case simulates a fading of 3.63 milliseconds but only half of each word would be affected).

Case IV: All bits in the first one-third of each word have equal probability p, all bits in the next one-third of each word have equal probability q, and all bits in the last one-third of each word have equal probability r. The relationship between the probabilities was chosen as $q = 3p/4$ and $r = \frac{1}{2}p$. (This case simulates a fade length of about 1 millisecond.)

Finally, we make a comparison of the Binary Union Decoder with the Simple Word Recognition Decoder. The Word Recognition Decoder gives an output signal only after it has recognized the received bit pattern as a valid word. Again we consider MILES block code words with weight W and N+1 repeated word transmissions. The special cases considered here are the following:

Case V: All bits in each word have equal probability p.

Case VI: All bits in the first half of the word have equal probability p and all bits in the second half have equal probability q, where $q = 3p/4$.

Case VII: One-third of the bits of each code word has probability p, one-third has probability q and one-third has probability r. We again assume $q = 3p/4$ and $r = \frac{1}{2}p$.

A. Case I - All Bits Equal Probability:

The bits of a single OR'ed word, which we will call A_i, are represented by the symbol α_{ij} where i denotes the bit number and j denotes the repeated word number. It then follows that, for example,

$$\alpha_{11} = a_{1,1} \cup a_{2,1} ,$$

$$\alpha_{12} = a_{1,2} \cup a_{2,2} , \tag{6.1}$$

while in general

$$\alpha_{1j} = a_{1,j} \cup a_{2,j} ,$$

$$\alpha_{2j} = a_{2,j} \cup a_{3,j} ,$$
$$\cdots\cdots\cdots$$
$$\alpha_{ij} = a_{i,j} \cup a_{i+1,j} , \qquad (6.2)$$

where $1 \leq i \leq N$ and $1 \leq j \leq W$. The letter N denotes the number of unions and thus N+1 is the number of repeated words transmitted, and the letter W is the weight of the code word (i.e., the number of "ones"). Now if only one good word is required for a successful decode (i.e., hit), then mathematically we wish to determine the probability associated with N unions of the "A's",

$$P(A_1 \cup A_2 \cup \ldots \cup A_N) = P(\bigcup_{i=1}^{N} A_i), \qquad (6.3)$$

where each A_i denotes a word of weight W. By considering only the "ones" and not the "zeros", we are considering only the fading loss and not the more general case of noise which could change a "zero" to a "one" as well as a "one" to a "zero".

If we first treat the special case of only three repeated words being transmitted, then we will be interested in computing

$$P(A_1 \cup A_2) = P(A_1) + P(A_2) - P(A_1 \cap A_2). \qquad (6.4)$$

In terms of the OR'ed bits α_{ij}, the intersection in (6.4) is

$$A_1 \cap A_2 = (\alpha_{11} \cap \alpha_{12} \cap \ldots \cap \alpha_{1W}) \cap (\alpha_{21} \cap \alpha_{22} \cap \ldots \cap \alpha_{2W}), \qquad (6.5)$$

or by regrouping,

$$A_1 \cap A_2 = (\alpha_{11} \cap \alpha_{21}) \cap (\alpha_{12} \cap \alpha_{22}) \cap \ldots \cap (\alpha_{1W} \cap \alpha_{2W}), \qquad (6.6)$$

and hence

$$P(A_1 \cap A_2) = \prod_{j=1}^{W} P(\alpha_{1j} \cap \alpha_{2j}). \qquad (6.7)$$

If each bit $a_{i,j}$ of the received word has probability p, it follows that the probability of each OR'ed bit α_{ij} is

$$P(\alpha_{ij}) = P(a_{i,j}) + P(a_{i+1,j}) - P(a_{i,j})P(a_{i+1,j})$$

$$= 1 - (1 - p)^2, \qquad (6.8)$$

and therefore the entire OR'ed word composed of the OR'ed bits α_{ij} is

$$P(A_i) = \left[1 - (1-p)^2\right]^W = \left[1 - (1-p)(1-p)\right]^W \qquad (6.9)$$

for i = 1,2. Also, we now see that

$$P(\alpha_{1j} \cap \alpha_{2j}) = P(\alpha_{1j}) + P(\alpha_{2j}) - P(\alpha_{1j} \cup \alpha_{2j})$$

$$= 2\left[1-(1-p)^2\right] - (3p-3p^2+p^3)$$

$$= 1 - (1-p)(1-p^2), \qquad (6.10)$$

and hence the union $A_1 \cup A_2$ has probability

$$P(A_1 \cup A_2) = 2\left[1-(1-p)(1-p)\right]^W - \left[1-(1-p)(1-p^2)\right]^W$$

which can be expressed in the equivalent form

$$P(A_1 \cup A_2) = \sum_{m=1}^{2} (-1)^{m+1} \binom{2}{m} \left[1-(1-p)(1-p^2)\right]^W$$

The symbols $\binom{k}{m}$ are binomial coefficients defined by

$$\binom{k}{m} = \frac{k!}{m!(k-m)!} \quad . \tag{6.12}$$

With the above special case serving as a model, we can now generalize the results to the case when N+1 repeated words are transmitted. Here we find the probability of successful decoding one word out of N+1 received is

$$P\left(\bigcup_{j=1}^{N} A_i\right) = S_1 - S_2 + S_3 - \ldots + (-1)^{N+1} S_N \tag{6.13}$$

where the S terms are

$$S_1 = \sum_{i=1}^{N} P(A_i) = \binom{N}{1}\left[1-(1-p)(1-p)\right]^W$$

$$S_2 = \sum_{\substack{i,j=1 \\ i \neq j}}^{N} P(A_i \cap A_j) = \binom{N}{2}\left[1-(1-p)(1-p^2)\right]^W$$

$$S_3 = \sum_{\substack{i,j,k=1 \\ i \neq j \neq k}}^{N} P(A_i \cap A_j \cap A_k) = \binom{N}{3}\left[1-(1-p)(1-p^3)\right]^W$$

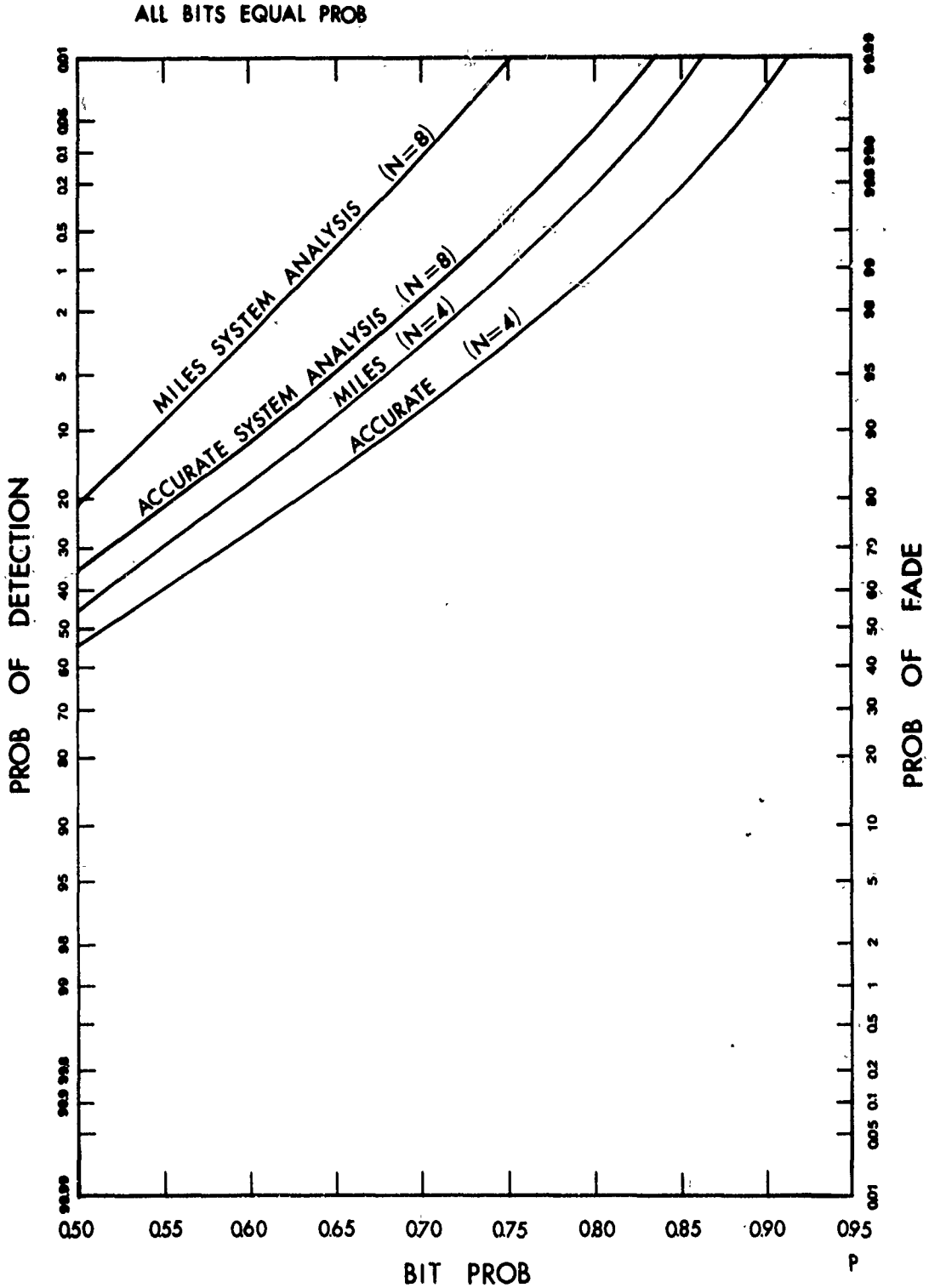

Fig. 6-2. Probability of detection curves for the case when all bits have equal probability and N = 4 or N = 8. The upper curve for each N corresponds to the previous MILES analysis given by Eq. (6.15) and the lower curve for each N corresponds to the present analysis based on Eq. (6.14).

. . . . . .

$$S_m = \sum_{\substack{i,\ldots,k=1 \\ i\neq\ldots\neq k}}^{N} P(A_i \cap \ldots \cap A_k) = \binom{N}{m}[1-(1-p)(1-p^m)]^W. \qquad m \text{ terms}$$

Hence the probability we seek is given by

$$P\left(\bigcup_{i=1}^{N} A_i\right) = \sum_{m=1}^{N} (-1)^{m+1} \binom{N}{m}[1-(1-p)(1-p^m)]^W. \qquad (6.14)$$

The above approach to the analysis is an accurate accounting of the Biary Union Decoder. It might be pointed out that if the unioned words, A_i, were assumed independent, as is the case in the current MILES analysis [21], the probability of a successful decode would be

$$P\left(\bigcup_{i=1}^{N} A_i\right) = 1 - \left\{1 - \left[1 - (1-p)^2\right]^W\right\}^{N+1}, \qquad (6.15)$$

where N+1 is again the number of repeated words and W is the weight of the word. A comparison of the probabilities generated by Eq.'s (6.14) and (6.15) is shown in Fig. 6-2. Here we see that the probabilities resulting from Eq. (6.15) are much higher than corresponding probalities given by Eq. (6.14), which are a direct result of ignoring the dependence of the unioned words A_i.

B. Case II - Half Word Fade Time

If we assume $a_{i,j}$ has probability p for j = 1...,W/2 and probability q for j = W/2 + 1,...,W, then Eq. (6.7) becomes

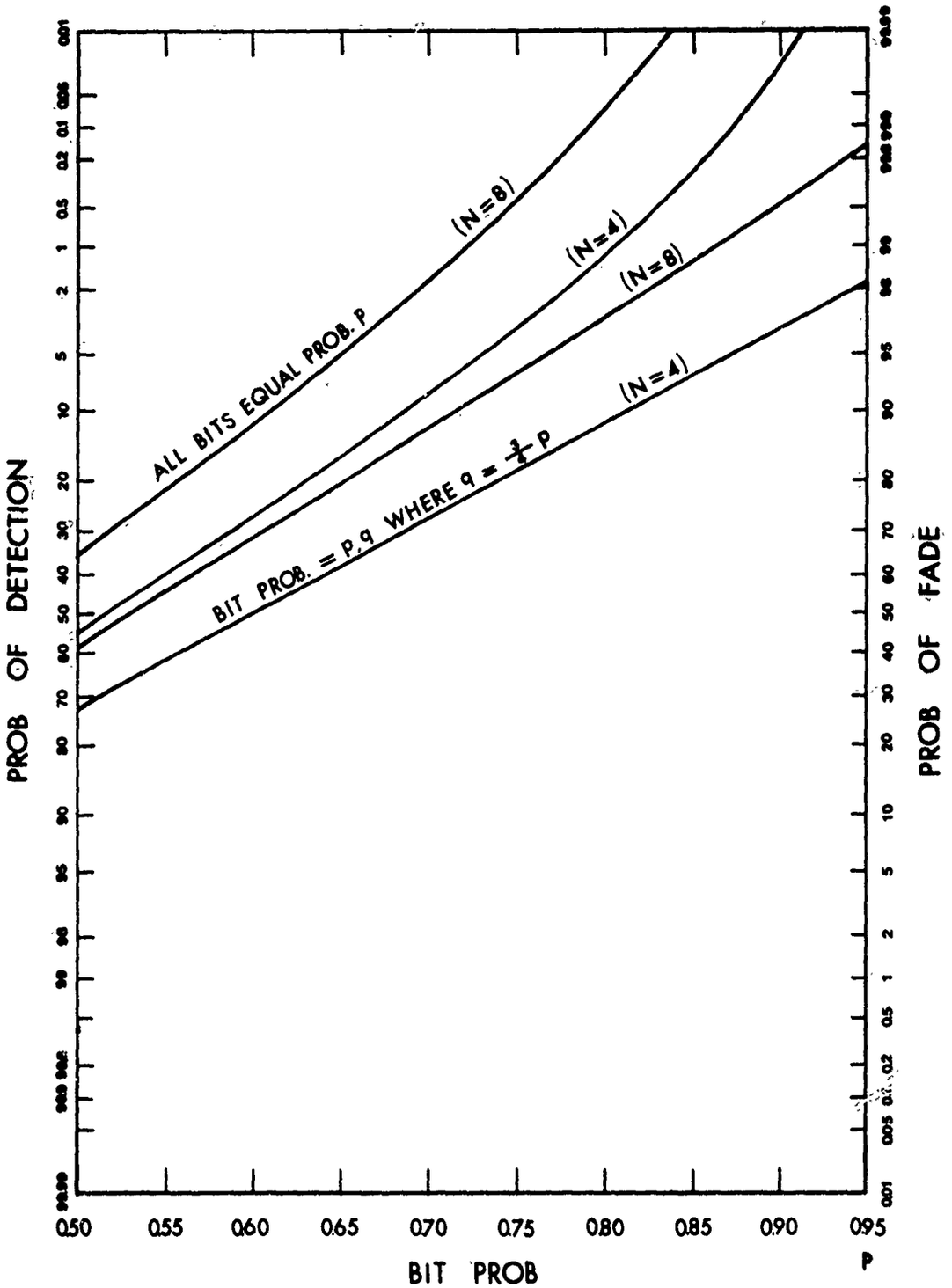

Fig. 6-3. Probability of detection curves (lower two) for the case when the first half word has probability p and the second half has probability q, and N = 4 or N = 8 (see Eq. (6.19)). The upper two curves correspond to the special case when all bits have equal probability p as given by Eq. (6.14).

$$P(A_1 \cap A_2) = \prod_{j=1}^{W/2} P(\alpha_{1j} \cap \alpha_{2j}) \prod_{j=\frac{W}{2}+1}^{W} P(\alpha_{1j} \cap \alpha_{2j}). \quad (6.16)$$

Using the result (6.10), we find

$$P(A_1 \cap A_2) = \left[1 - (1-p)(1-p)^2)\right]^{W/2} \left[1 - (1-q)(1-q^2)\right]^{W/2}, \quad (6.17)$$

and therefore it follows that

$$P(A_1 \cup A_2) = \sum_{m=1}^{2} (-1)^{m+1} \binom{2}{m} \left\{\left[1 - (1-p)(1-p^m)\right] \left[1 - (1-q)(1-q^m)\right]\right\}^{W/2}. \quad (6.18)$$

Generalizing Eq. (6.18), we have

$$P\left(\bigcup_{i=1}^{N} A_1\right) = \sum_{m=1}^{N} (-1)^{m+1} \binom{N}{m} \left\{\left[1-(1-p)(1-p^m)\right]\left[1-(1-q)(1-q^m)\right]\right\}^{W/2}. \quad (6.19)$$

Eq. (6.19) is plotted in Fig. 6-3 for the special case when the bit probabilities satisfy $q = 3p/4$ and $N = 4$ or $N = 8$. Corresponding curves for the case when all bits have probability p (see Eq. (6.14)) are illustrated here for comparison purposes. The relative bit probabilities chosen were picked only as typical of fading conditions and also to demonstrate the effect of the Binary Union on the word detection probability.

C. Case III - Full Word Fade Time - Half Word Lost:

Here we assume $P(a_{1,j}) = p$, $j = 1,\ldots,W/2$ and $P(a_{1,j}) = q$, $j = W/2 +1,\ldots,W$. Then $P(a_{2,j}) = q$, $j = 1,\ldots,W/2$ and $P(a_{2,j}) = p$, $j = W/2 +1,\ldots,W$, and so on where every other word has the same probabilities assigned to each bit.

For three repeated words, we must calculate

$$P(A_1 \cup A_2) = P(A_1) + P(A_2) - P(A_1 \cap A_2), \tag{6.20}$$

where

$$P(A_1) = \prod_{j=1}^{W/2} P(\alpha_{1j}) \prod_{j=\frac{W}{2}+1}^{W} P(\alpha_{1j})$$

$$= (p + q - pq)^{W/2} \quad (q + p - qp)^{W/2}$$

$$= [1 - (1-q)(1-p)]^{W}, \tag{6.21}$$

and likewise

$$P(A_2) = [1 - (1-q)(1-p)]^{W}. \tag{6.22}$$

Also, we find that

$$P(A_1 \cap A_2) = \bigcap_{j=1}^{W/2} P(\alpha_{1j} \cap \alpha_{2j}) \bigcap_{j=\frac{W}{2}+1}^{W} P(\alpha_{1j} \cap \alpha_{2j})$$

$$= [2(p+q-pq)-(2p+q-2pq-p^2+p^2q)]^{W/2} [2(p+q-pq)-(2q+p-2pq-q^2+pq^2)]^{W/2}$$

$$= [1 - (1-q)(1-p^2)]^{W/2} [1 - (1-p)(1-q^2)]^{W/2}. \tag{6.23}$$

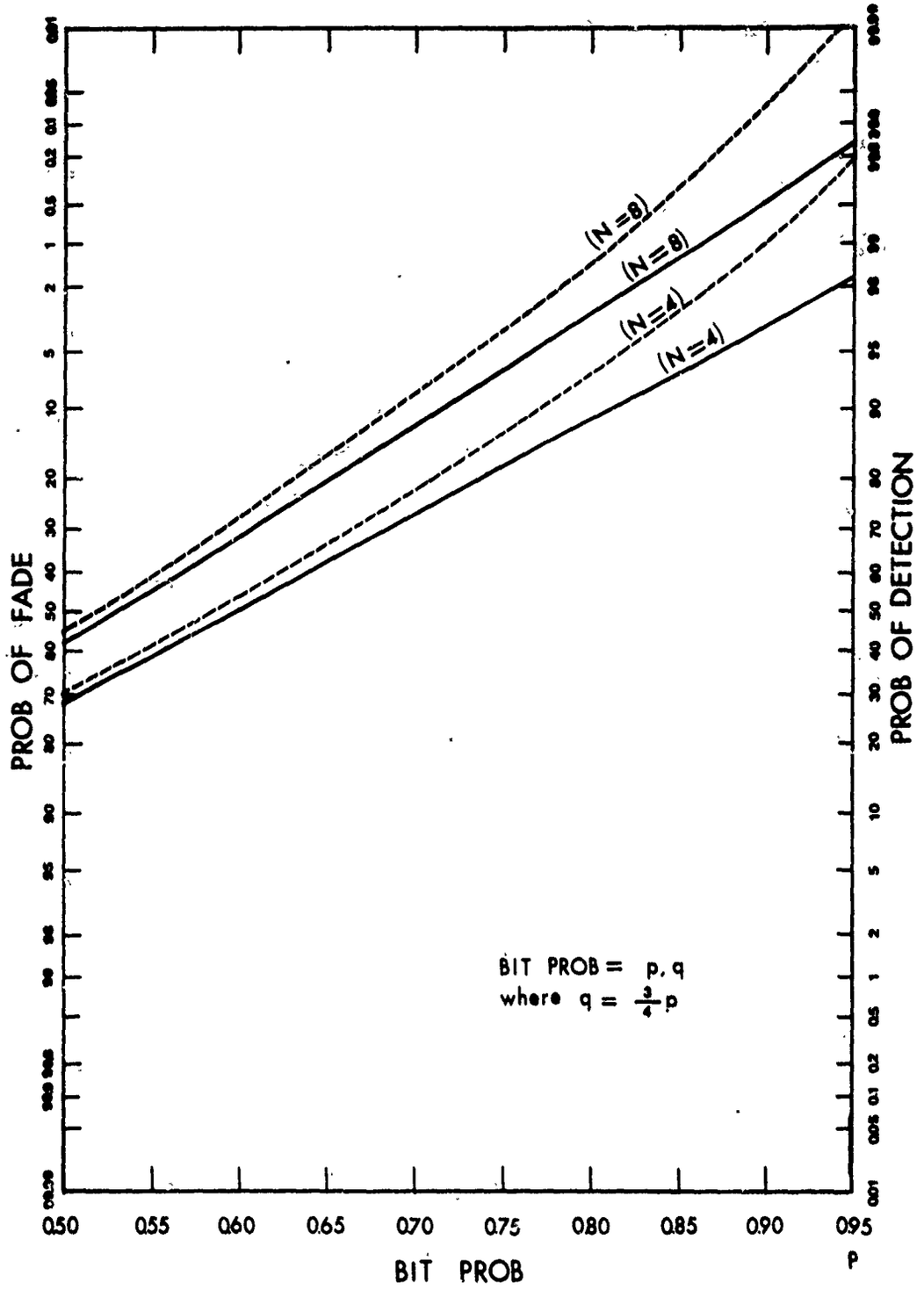

Fig. 6-4. Probability of detection curves for the case when the first half of every other word has probability p and the second half has probability q, alternated with those words where the first half has probability q and the second half has probability p, and N = 4 or N = 8 (see Eq. (6.25)). The dashed curve for each N corresponds to the probability of detection when each word has the same p,q probability assignment as the previous word (see Eq. (6.19)).

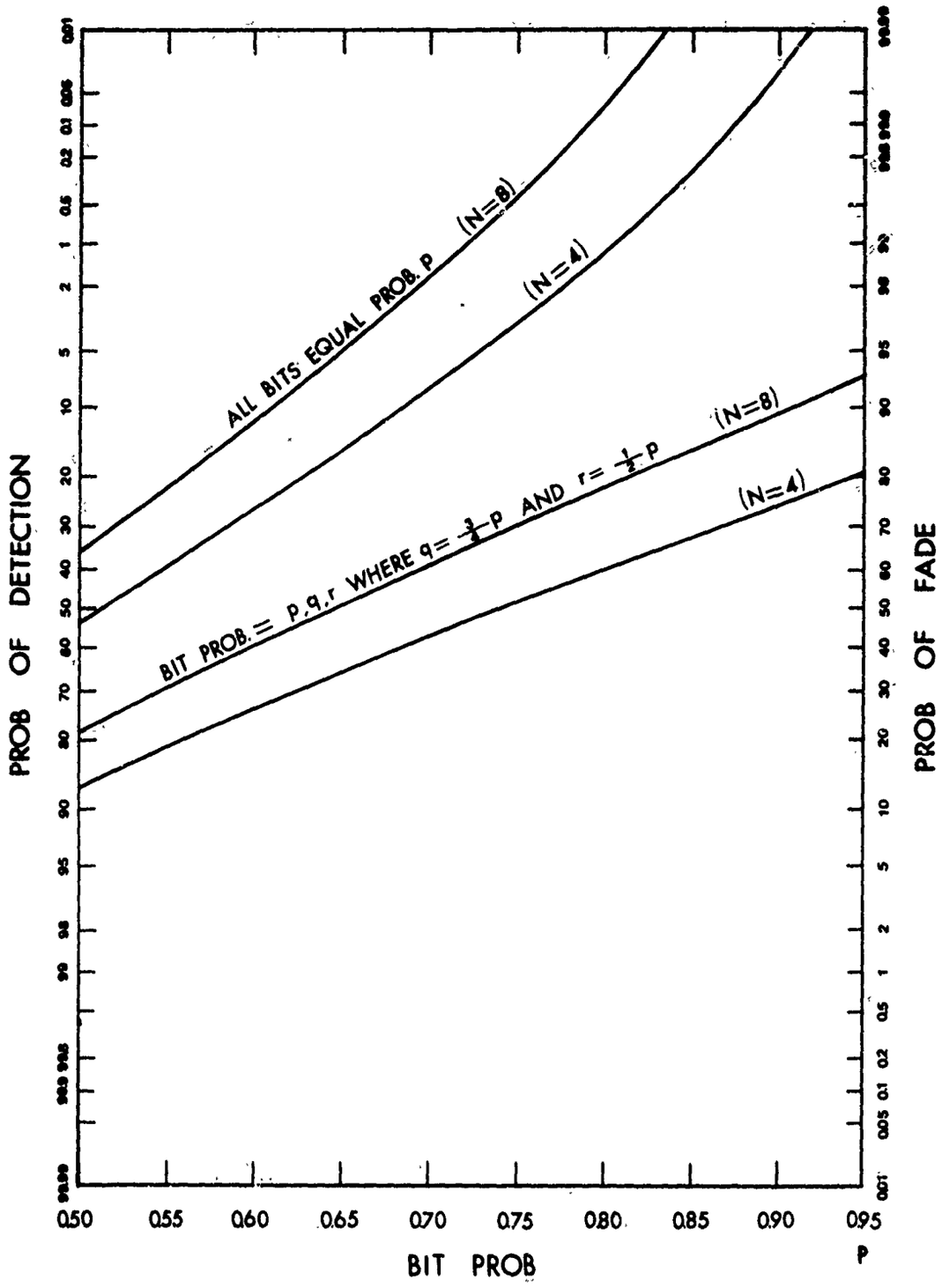

Fig. 6-5. Probability of detection curves for the case when the first one-third of the word has probability p, the next one-third has probability q, and the last one-third has probability r, where $q=3p/4$ and $r=\frac{1}{2}p$, and N = 4 or N = 8 (see Eq. (6.26)). The upper two curves correspond to the special case when all bits have equal probability p as given by Eq. (6.14)).

Therefore, Eq. (6.20) now takes the form

$$P(A_1 \quad A_2) = \sum_{m=1}^{2} (-1)^{m+1} \binom{2}{m} \{[1-(1-q)(1-p^m)] \; [1-(1-p)(1-q^m)]\}^{W/2}, \qquad (6.24)$$

and generalizing to N+1 repeated words yields

$$P(\bigcup_{i=1}^{N} A_i) = \sum_{m=1}^{N} (-1)^{m+1} \binom{N}{m} \{[1-(1-q)(1-p^m)] \; [1-(1-p)(1-q^m)]\}^{W/2}. \qquad (6.25)$$

Probability of detection curves using Eq. (6.25) for the special case when $q = 3p/4$ and $N = 4$ or $N = 8$ are shown in Fig. 6-4. The upper curves for each N illustrate similar probabilities of detection when each word has the same probabilities p and q as determined by Eq. (6.19), rather than every other word as is the case of present interest.

D. Case IV - Third of a Word Faded:

Finally we consider when $P(a_{i,j}) = p$, $j = 1,\ldots,W/3$, $P(a_{i,j}) = q$, $j = W/3+1,\ldots,2W/3$, and $P(a_{i,j}) = r$ for $j = 2W/3+1,\ldots,W$. Following the same procedure as outlined in Section B, we find that

$$P(\bigcup_{i=1}^{N} A_i) = \sum_{m=1}^{N} (-1)^{m+1} \binom{N}{m} \{[1-(1-p)(1-p^m)] \; [1-(1-q)(1-q^m)] \; [1-(1-r)(1-r^m)]\}^{W/3}. \qquad (6.26)$$

Probability of detection curves for this case are illustrated in Fig. 6-5 for the special case when $q = 3p/4$ and $r = \frac{1}{2}p$. Again these values represent typical probabilities.

E. Case V - All Bits Equal Probability:

If we let the probability of detection of a single bit be p, the

word detection probability for a word of weight W is

$$P_{word} = p^W. \tag{6.27}$$

The probability of missing a word is

$$P_M = 1 - p^W \tag{6.28}$$

and the probability of missing every one of N+1 repeatedly transmitted words is

$$P_{MW} = (1 - p^W)^{N+1}. \tag{6.30}$$

F. Case VI - One Half Word Fade:

Suppose p is the probability of detecting half of the bits in a word and q is the probability of detecting the second half of the bits in the same word. The probability of detecting the word is

$$P_{word} = p^{W/2} q^{W/2}, \tag{6.31}$$

and hence the probability of detecting one word in N+1 repeated transmissions is

$$P_D = 1 - [1 - (pq)^{W/2}]^{N+1}. \tag{6.32}$$

G. Case VII - One-Third of a Word Faded:

Let the probability of each third of a word be p, q, and r, respectively. Following the analysis in Section F, we deduce that the probability of detecting a single word when N+1 are transmitted is

$$P_D = 1 - [1 - (pqr)^{W/3}]^{N+1}. \qquad (6.33)$$

Fig. 6-6 shows the plots of Eq.'s (6.30), (6.32) and (6.33) where we have chosen $q = 3p/4$ and $r = \frac{1}{2}p$. These choices represent typical fading depths and rates as discussed earlier. Comparison of the results here for the Word Recognition Decoder and those in previous sections for the Binary Union Decoder clearly reveals the effectiveness of the Binary Union Decoder. Observe, however, that the Binary Union Decoder is most effective by comparison with the Word Recognition Decoder when all bits have equal probability.

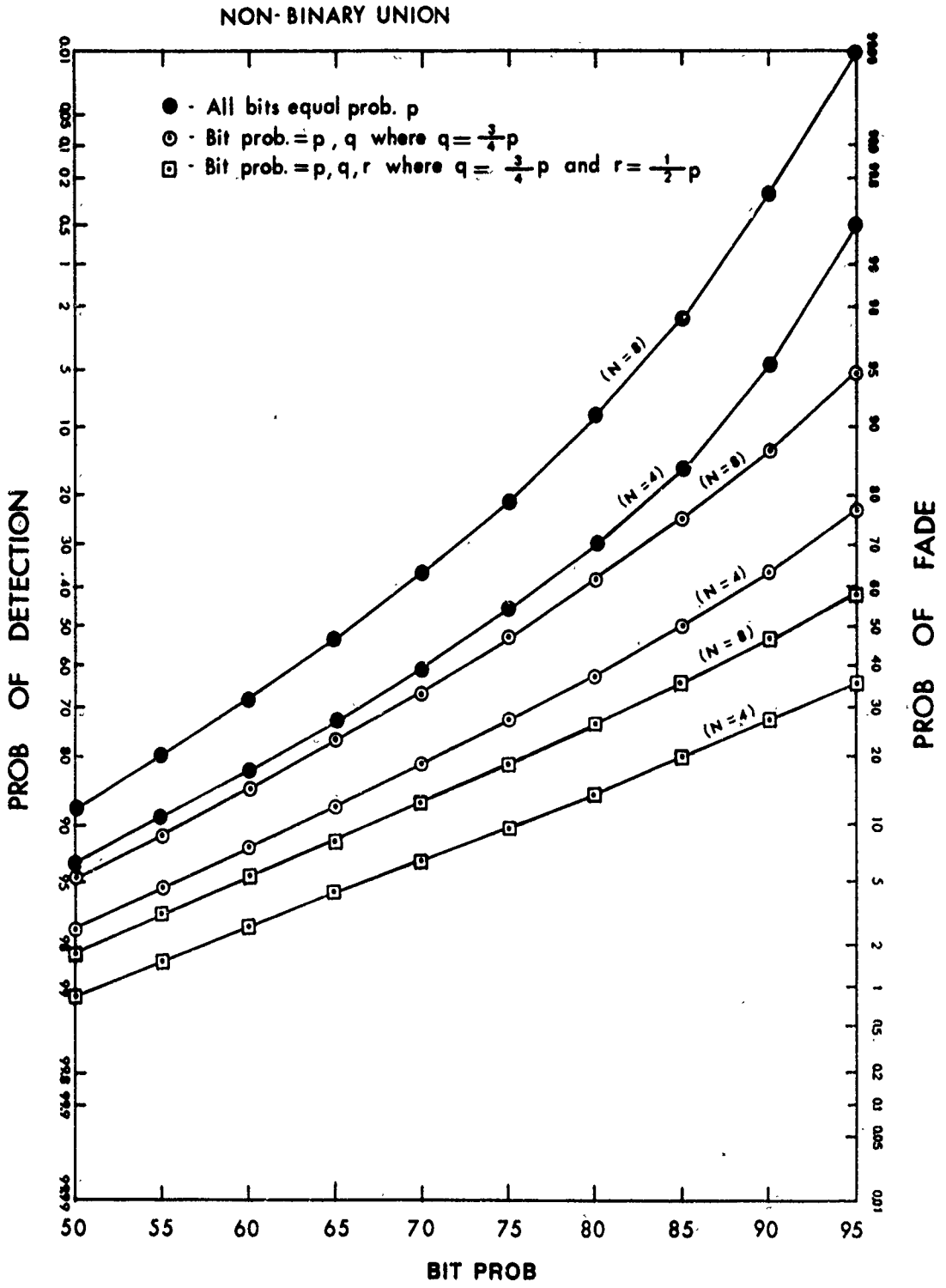

Fig. 6-6. Probability of detection curves for the Word Recognition Decoder corresponding to either N = 4 or N = 8. The upper two curves correspond to Eq. (6.30) where all bits have equal probability, the middle two curves correspond to that case when half the received word has probability p and half has probability q (Eq. (6.32)), and the lower two curves correspond to that case when the word probability is split into thirds (Eq. (6.33)).

VII. DISCUSSION

The purpose of this study was to evaluate the potential for using MILES equipment for long range marksmanship gunnery training. The current MILES equipment was designed as a tactical engagement laser weapon fire simulator. In the development of the system detailed analysis was performed to predict the optical communication process. The Binary Union Decoder was designed to increase the detection probability of received MILES words under very specific fading conditions. That analysis was performed assuming short range propagation path and weak scattering in the path. Also, simplifications were made in the analysis of the MILES decoder circuit which are valid for the short range problem but which proved unreliable and misleading for the long range problem. That is, if the short range (200 meters) analysis is extended to the longer ranges the probability of detection curves that result are overly optimistic.

In order to definitively evaluate the MILES potential for long range marksmanship gunnery training, the following tasks are required:

1. Evaluate currently available mathematical models and alter or create new models for long range optical propagation.
2. Experimentally evaluate MILES long range detection probability (kill probability).
3. Develop appropriate and necessary add-ons for MILES equipment which will allow it to accurately simulate long range gun firing for marksmanship training.

A. Completed Modelling Tasks:

During the current study we have completed the following aspects of the mathematical modelling:

(a). Experimentally determined, in well documented field experiments, conducted at NASA's Kennedy Space Center, that the Lognormal Statistical Model for scintillation scattering is valid only for ranges less than 200 meters (or weak turbulence conditions).

(b). The field experiments also proved that the variance of the statistically fluctuating optical signal at long ranges does not saturate at the low values (0.7) used in the MILES analysis. The actual variance at long ranges may be as high as 4 or 5.

(c). The K-distribution was validated as a reasonable model for long ranges although it is not theoretically applicable for short ranges when the normalized variance is less than unity.

(d). The cumulative fading (or cumulative distribution) was computed for the K-distribution and for the lognormal distribution using the same variance in both cases (see Fig. 7-1). The lognormal model predicts lower fading at long ranges as compared with the K-distribution leading to a more optimistic view of system performance.

(e). A universal statistical model, called the G-distribution, was developed that would accurately predict scattering effects at both short range and long range. Due to complexities of the mathematical functional form of the G-distribution, only the statistical moments have been computed with the distribution at this time. Further analysis and refinement of this distribution is required

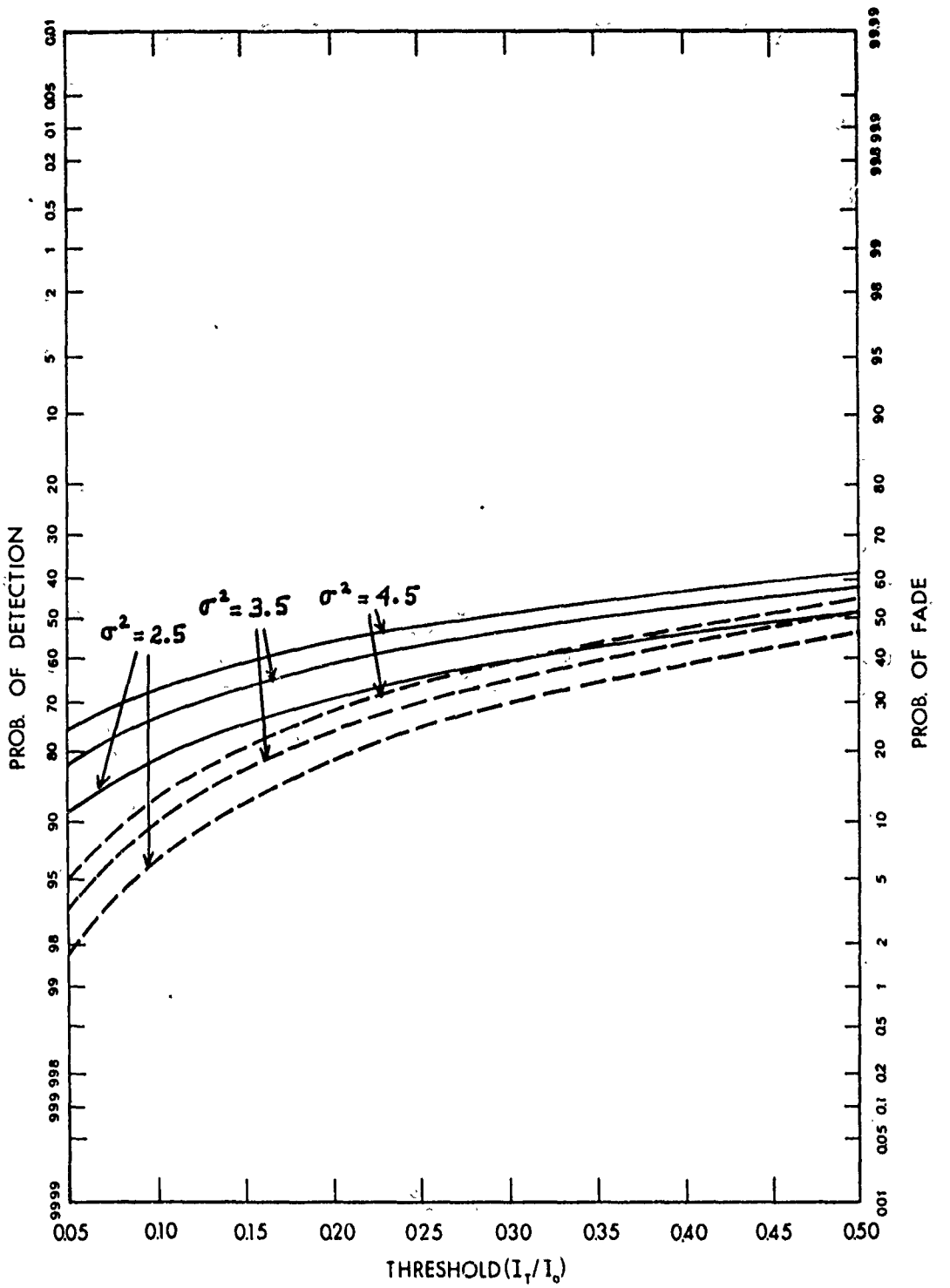

Fig. 7-1. Comparison of cumulative fading model for K-distribution (solid curves) and lognormal distribution (dashed curves) as a function of the ratio of receiver threshold to mean intensity.

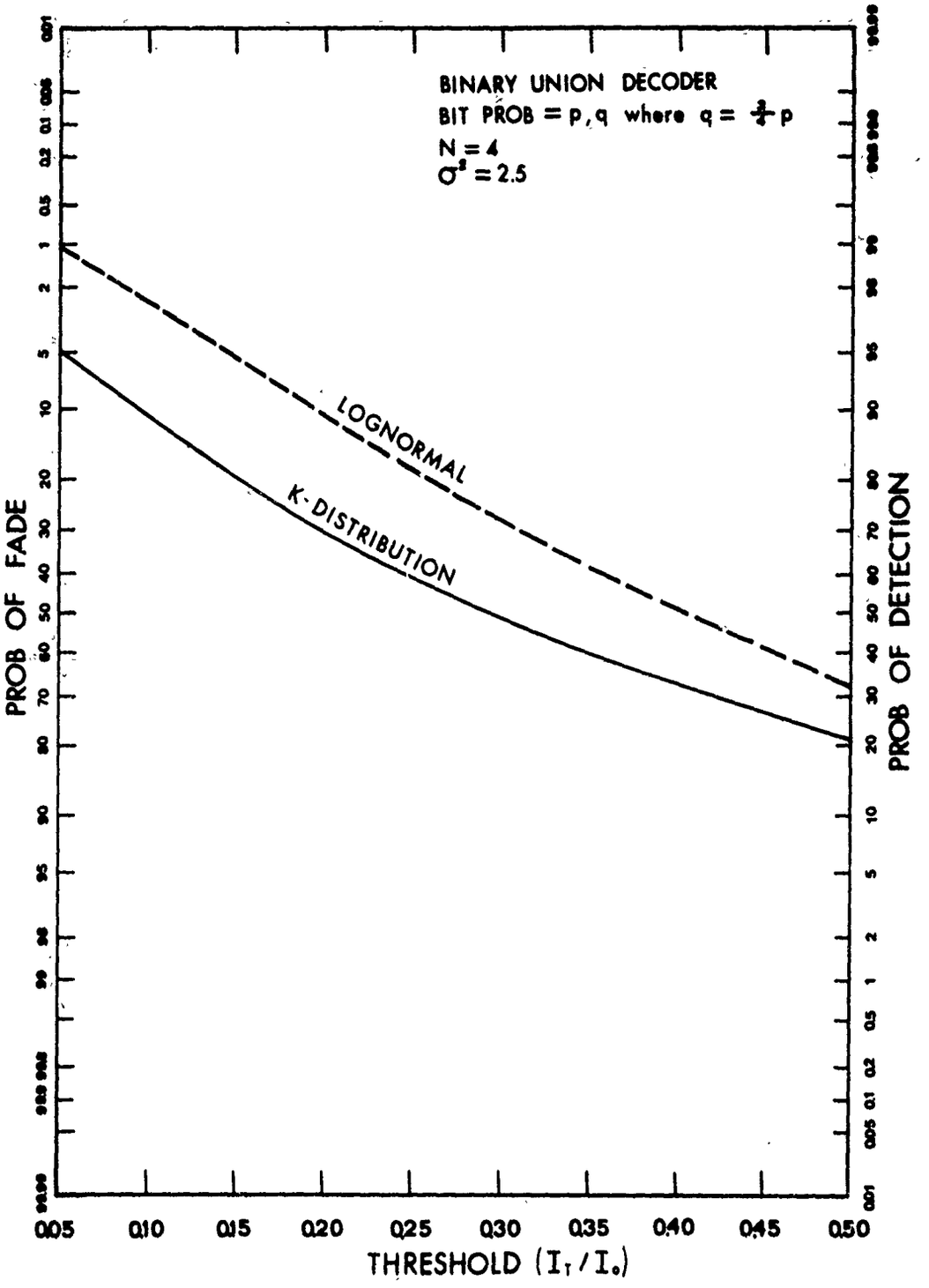

Fig. 7-2. Comparison of word detection probabilities of Binary Union Decoder for K-distribution and lognormal distribution fading models.

to cast it into a form that will be propitious to the computation of cumulative fading.

In addition to the mathematical modelling of the intensity fluctuations of the optical beam, an analysis was performed on the Binary Union Decoder employed in the MILES system. Although the current analysis was reasonably accuracy for short ranges [21], it leads to a considerably over-optimistic performance of the MILES system for longer ranges. The analysis performed in this study for the decoder made use of the lognormal distribution as well as the K-distribution to illustrate the differences in the predicted performance of MILES at long ranges for both statistical models (see Fig. 7-2).

B. Evaluation of MILES Equipment:

As of the completion of this portion of the study, there has been no MILES equipment available for testing. If and when the equipment becomes available, it will be taken to NASA's Space Shuttle Runway for the purpose of conducting experiments in the hopes of determining detection (kill) probability zones as a function of range.

C. MILES Equipment Add-On:

The major portion of the marksmanship study concerning MILES hardware add-ons was conducted by Code N-73 of NTEC's research division. The UCF research team worked with Code N-73 in the early stages of the study to help develop add-on hardware concepts that would be MILES compatible and allow MILES to be used in marksmanship gunnery training. The concepts that evolved from the preliminary discussions were:

1. Phase locked loop (PLL) receiver.

2. Digital filter (DF) receiver.

3. Continuous wave (CW) laser, transmitter pulsed at high rate.

Since the MILES transmitters operate at a basic transmission rate of 3 khz, the high pulse rate CW laser could be configured so as to transmit 20 pulses during the slot time for one MILES bit pulse. The receivers would then lock onto the 20 pulses and output one pulse at the MILES bit pulse period. Hence the proposed transmitter and receiver would appear as standard MILES transmitter and receiver to the present MILES encoder and decoder electronic systems. In order to drive the transmitter and receiver developed by Code N-73 of NTEC, the UCF research team developed the software so that the microprocessor system PROMPT 80 could be used as MILES encoder. The MILES decoder system can be simulated using the MINC-11 computer. Appendix C lists the microprocessor program for simulating the MILES encoder.

The above techniques were being developed simultaneously and in conjunction with the UCF study of the mathematical modelling. These techniques are well known in communication theory and appear to be very promising as techniques to allow MILES to be used for marksmanship gunnery training.

APPENDIX A

The Characteristic Function

Let us write the time-independent portion of the field as

$$E = Ae^{i\theta} + Re^{i\phi} = E_1 + E_2. \tag{A-1}$$

Since E_1 and E_2 are complex functions, we define their characteristic functions as two-dimensional Fourier transforms. For E_1, this becomes

$$C_1(u,v) = \int_0^{\infty} \int_0^{2\pi} e^{iuA\cos\theta + ivA\sin\theta}\, p(A,\theta)\, d\theta dA, \tag{A-2}$$

where $p(A,\theta)$ is the joint density function of A and θ. If we assume that A and θ are independent, and further that θ is uniformly distirbuted, then

$$p(A,\theta) = p(A)p(\theta) = \frac{1}{2\pi}\, p(A)$$

and (A-2) can be written in the form

$$c_1(u,v) = \int_0^{\infty} p(A)\, \frac{1}{2\pi} \int_0^{2\pi} e^{iAz\cos(\theta - \alpha)}\, d\theta\, dA, \tag{A-3}$$

where

$$z = \sqrt{u^2 + v^2}$$

and

$$\alpha = \arctan(v/u).$$

Using the integral formula ([17], p. 360)

$$\frac{1}{2\pi} \int_0^{2\pi} e^{ix\cos\phi}\, d\phi = J_o(x) \tag{A-4}$$

it becomes clear that C_1 depends only upon the radial variable z, i.e.,

$$C_1(z) = \int_0^{\infty} p(A)J_o(Az)\, dA, \tag{A-5}$$

which we recognize as being equivalent to the Hankel transform of $p(A)/A$. Under similar assumptions for R and ϕ, the characteristic function for E_2 leads to

$$C_2(z) = \int_0^\infty p(R)J_o(Rz)\, dR\ , \tag{A-6}$$

and therefore the characteristic function for $E = E_1 + E_2$ can be expressed in the product form

$$C(z) = C_1(z)C_2(z) = \int_0^\infty p(A)J_o(Az)dA \int_0^\infty p(R)J_o(Rz)dR. \tag{A-7}$$

The pdf for E is defined as the two-dimensional Fourier transform of $C(z)$ given by

$$p(E) = \frac{1}{4\pi^2} \int_{-\infty}^{\infty}\int_{-\infty}^{\infty} e^{-iuX - ivY}\, C(z)\, du\, dv, \tag{A-8}$$

where

$$X = Re(E) = A\cos\theta + R\cos\phi$$

and

$$Y = Im(E) = A\sin\theta + R\sin\phi.$$

Since the characteristic function is formulated in terms of the radial variable z it is convenient to write the exponential function in (A-8) in terms of polar coordinates. Thus we write

$$uX + vY = |E|z\cos(\psi - \alpha)$$

where

$$|E| = \sqrt{X^2 + Y^2}$$

and

$$\psi = \arctan(Y/X).$$

Converting the double integral in (A-8) to polar coordinates (z,α) it follows that

$$p(E) = \frac{1}{4\pi^2} \int_0^\infty \int_0^\infty zC(z)e^{-i|E|z\cos(\psi - \alpha)}\, d\alpha\, dz \tag{A-9}$$

which in view of (A-4) further reduces to

$$p(E) = \frac{1}{2\pi}\int_0^\infty zC(z)J_o(|E|z)\,dz \qquad \text{(A-10)}$$

Now since

$$p(E) = p(|E|)p(\psi) = \frac{1}{2\pi}\,p(|E|),$$

we see that

$$p(|E|) = \int_0^\infty zC(z)J_o(|E|z)\,dz, \qquad \text{(A-11)}$$

and finally, by making the transformation $I = |E|^2$, we obtain the pdf for the intensity I,

$$p(I) = \tfrac{1}{2}\int_0^\infty zC(z)J_o(\sqrt{I}z)\,dz. \qquad \text{(A-12)}$$

APPENDIX B

The Meijer G-Function

In Section VA we developed the expression

$$p(I) = \sum_{k=0}^{\infty} \frac{(-1)^k \langle A^{2k} \rangle}{(k!)^2 \Gamma(m)} I^{-(k+1)} \, G_{23}^{21}\left(\frac{mI}{b} \middle| \begin{matrix} 1, & 1 \\ k+1, & m, \quad k+1 \end{matrix} \right) \tag{B-1}$$

as the pdf associated with the intensity fluctuations of an optical beam propagating through clear-air turbulence. By $G_{23}^{21}(.)$, we mean one member of the generalized function known as the Meijer G-function [19]. It is our intent here to relate this function to more standard functions used in engineering applications. In particular, we will show that $G_{23}^{21}(.)$ is related to the generalized Laguerre functions.

Using the relations ([19], vol. 1, p. 209 and p. 216)

$$G_{23}^{21}\left(x \middle| \begin{matrix} \alpha, & a \\ b, & c, \quad \alpha \end{matrix} \right) = G_{12}^{20}\left(x \middle| \begin{matrix} a \\ b, & c \end{matrix} \right) \tag{B-2}$$

and

$$G_{12}^{20}\left(x \middle| \begin{matrix} a \\ b, & c \end{matrix} \right) = x^{\frac{1}{2}(b+c-1)} \, e^{-\frac{1}{2}x} \, W_{\frac{1}{2}(b+c+1)-a, \, \frac{1}{2}(b-c)}(x), \tag{B-3}$$

we can relate a particular $G_{23}^{21}(.)$ function to the Whittaker functions $W_{\mu,\nu}(.)$. Then employing the relation ([19]. vol. 2, p. 432)

$$W_{\mu+n+\frac{1}{2}, \, \pm\mu}(x) = (-1)^n \, n! \, x^{\mu+\frac{1}{2}} \, L_n^{(2\mu)}(x) \, e^{-x/2}, \tag{B-4}$$

where $L_n^{(\alpha)}(.)$ is the generalized Laguerre function, we have one special case of interest

$$G_{23}^{21}\left(x \middle| \begin{matrix} \alpha, & a \\ b, & c, \quad \alpha \end{matrix} \right) = (-1)^{b-a} \, (b-a)! \, x^c \, e^{-x} \, L_{b-a}^{(c-b)}(x). \tag{B-5}$$

The G-function in (B-1) is more general than that in (B-5). Therefore in order to utilize (B-5) we need to develop an appropriate recurrence-type formula which relates the more general G-function to those of the specific form in (B-5). Such a recurrence formula can be derived by making use of the relation

$$G_{23}^{21}\left(x\left|\begin{matrix} n,\ 1 \\ k+j,\ m,\ k+1 \end{matrix}\right.\right) = (k+j-n)G_{23}^{21}\left(x\left|\begin{matrix} n+1,\ 1 \\ k+j,\ m,\ k+1 \end{matrix}\right.\right) - G_{23}^{21}\left(x\left|\begin{matrix} n+1,\ 1 \\ k+j+1,m,k+1 \end{matrix}\right.\right) \quad \text{(B-6)}$$

which is a special case of Eq. (11), p. 209, vol. 1, [19]. Starting with $j = 1$ and $n = 1$, repeated application of (B-6) yields

$$G_{23}^{21}\left(x\left|\begin{matrix} 1,\ 1 \\ k+1,m,k+1 \end{matrix}\right.\right) = kG_{23}^{21}\left(x\left|\begin{matrix} 2,1 \\ k+1,m,k+1 \end{matrix}\right.\right) - G_{23}^{21}\left(x\left|\begin{matrix} 2,\ 1 \\ k+2,m,k+1 \end{matrix}\right.\right)$$

$$= k(k-1)G_{23}^{21}\left(x\left|\begin{matrix} 3,\ 1 \\ k+1,m,k+1 \end{matrix}\right.\right) - 2kG_{23}^{21}\left(x\left|\begin{matrix} 3,\ 1 \\ k+2,m,k+1 \end{matrix}\right.\right)$$

$$+ G_{23}^{21}\left(x\left|\begin{matrix} 3,\ 1 \\ k+3,m,k+1 \end{matrix}\right.\right) ,$$

. . . . . .

while in general it can be shown that

$$G_{23}^{21}\left(x\left|\begin{matrix} 1,\ 1 \\ k+1,\ m,\ k+1 \end{matrix}\right.\right) = \sum_{j=0}^{k} (-1)^{k-j} \binom{k}{j}^2 j!\, G_{23}^{21}\left(x\left|\begin{matrix} k+1,\ 1 \\ 2k-j+1,m,k+1 \end{matrix}\right.\right) . \quad \text{(B-7)}$$

Recalling (B-5), this last result leads to

$$G_{23}^{21}\left(x\left|\begin{matrix} 1,\ 1 \\ k+1,\ m,\ k+1 \end{matrix}\right.\right) = (-1)^k x^m e^{-x} \sum_{j=0}^{k} \binom{k}{j}^2 j!(2k-j)!L_{2k-j}^{(m-2k+j-1)}(x), \quad \text{(B-8)}$$

and the substitution of this expression with $x = mI/b$ into (B-1) gives us

$$p(I) = \frac{m^m I^{m-1}}{\Gamma(m)b^m} e^{-mI/b} \sum_{k=0}^{\infty} \sum_{j=0}^{k} \frac{(2k-j)!\langle A^{2k}\rangle}{j!\,[(k-j)!]^2} I^{-k} L_{2k-j}^{(m-2k+j-1)}(mI/b). \quad \text{(B-9)}$$

It may be of interest to consider here the separate case when $m = 1$ since (B-9) reduces to a result previously obtained through other means. From the relation ([18], p. 1038)

$$L_n^{(-n)}(x) = (-1)^n x^n/n!,$$

we find

$$I^{-k} \sum_{j=0}^{k} \frac{(2k-j)!}{j![(k-j)!]^2} L_{2k-j}^{(-2k+j)}(I/b) = b^{-k} \sum_{j=0}^{k} \frac{(-1)^j (I/b)^{k-j}}{j![(k-j)!]^2},$$

and by setting $k - j = n$,

$$I^{-k} \sum_{j=0}^{k} \frac{(2k-j)!}{j![(k-j)!]^2} L_{2k-j}^{(-2k+j)}(I/b) = \frac{(-1)^k}{b^k\, k!} \sum_{n=0}^{k} (-1)^n \binom{k}{n} \frac{(I/b)^n}{n!}$$

$$= \frac{(-1)^k}{b^k\, k!} L_k(I/b),$$

where $L_k(.)$ is the kth Laguerre polynomial. Thus, by setting $m = 1$ in (B-9) and using the above relation, we see that (B-9) reduces to

$$p(I) = \frac{1}{b} e^{-I/b} \sum_{k=0}^{\infty} \frac{(-1)^k \langle A^{2k} \rangle}{b^k\, k!} L_k(I/b) \qquad \text{(B-10)}$$

which is in agreement with Eq. (19) in [8] for $I = E^2$ and $b = 2\sigma_b^2$. That is to say, (B-10) is the pdf that would result under the assumption that the diffuse component(s) have an amplitude R that is Rayleigh distributed rather than the more general m-distribution as assumed for our model leading to (B-9).

APPENDIX C

Mircoprocessor Simulator

and High Data Rate Receiver

C.1 Transmitter and Encoder:

In order to conduct experiments on the high data concepts for MILES add-on's it is required that the MILES encoder-transmitter be simulated. The encoder transmitter design required that the system be as flexible as possible. This design had to allow for a variety of experiments on different types of modulation and block coding schemes. Because of the diversity of digital block codes, it was decided that a general purpose microprocessor computer should be used to generate these codes. The different proposed concepts also required that the transmitter be able to transmit block codes either by Frequency Shift Keying (FSK) or by On-Off Keying (OOK) modulation formats.

The use of a computer for generating block codes requires the computer to interface with a teletype and to have an I/O port that is easily accessible. The computer used for this task was the Prompt 80, an Intel 8080 (CPU) computer, which is capable of driving the necessary teletype and has an easily accessible I/O port. The Prompt 80 is limited to 1K of R.A.M. memory, but because it doesn't have an on-board assembler, programs must be hand-assembled and keyed in by hand via the front panel keyboard.

The code generation program had to produce block codes that were MILES compatible. The MILES block codes consist of 32 different 11-bit words. These words are sent at a bit rate of 333 μ sec per bit. Each word is then repeated and re-transmitted a specified number of times. For the Dragon missle, the Tow missle and the Viper, a special subroutine

was needed. To reduce the number of program subroutines required, the number of repeats of the word transmission was entered via the teletype. A Print subroutine, an ASC11 binary-to-binary subroutine, an ASC11 decimal-to-binary subroutine, and an output subroutine were the major subroutines written. The Print subroutine printed the messages on the teletype. The ASC11 binary-to-binary subroutine and the ASC11 decimal-to-binary subroutine were two required conversion routines. The ASC11 binary-to-binary subroutine was used to enter the 11-bit code word while the ASC11 decimal-to-binary subroutine was used to enter the number of times the code would be repeated. The maximum repetion of the code was set at 99. The output subroutine serially clocked the 11-bit code words bit by bit at a rate of 333 μ sec per bit. The program listing is given in Table C-1.

The output of the computer was used to control the modulator which in turn was used for the two different modulating formats (FSK and OOK). The circuit developed allowed for both methods to be utilized with a minimum number of components (see Fig. C-1), and switches from FSK to OOK by the throw of a switch. The modulator circuit performs in the following way. The flip-flop and nand gates 1 and 2 are used to divide the input carrier's frequency by two. These three logic devices allow the carrier's frequency to be divided by two and yet be independent of the carrier's pulse width (minimum of 60 nsec pulse width). With the switch closed, there is no output from nand gate 2 and hence its output remains low (0V). The computer code controls which carrier signal is allowed at the output of nand gate 6; this is accomplished with nand gates 3 and 5. If the computer output is low (0V), a high (+5V) appears at the input to nand gate 3 and a low (0V)

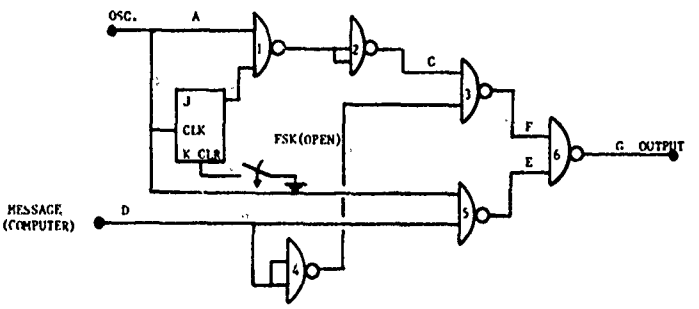

Fig. C-1(a). Modulator configuration for FSK and OOK modulation of MILES codes.

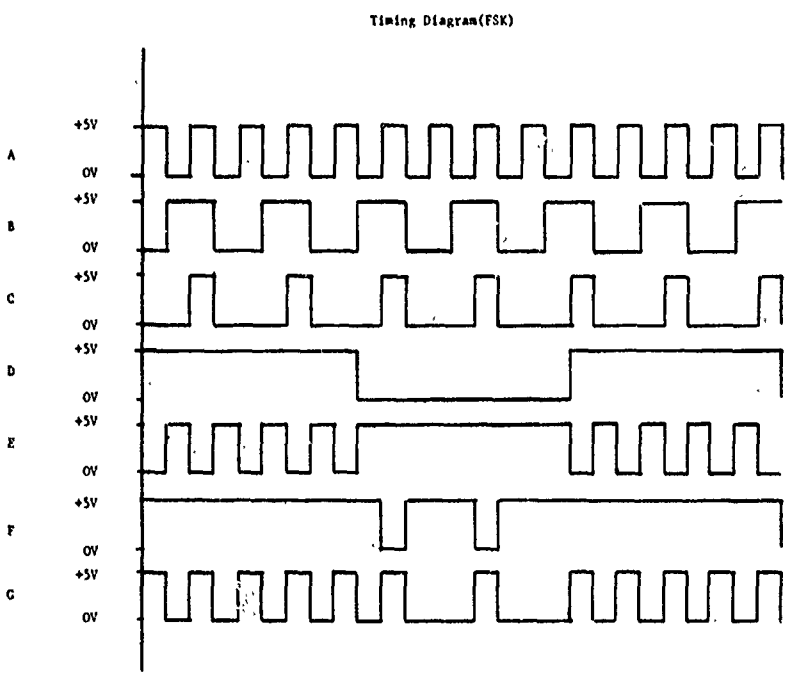

Fig. C-1(b). Timing diagram of modulator.

appears at the input to nand gate 5. A high (+5V) at the input to nand gate 3 allows the carrier (with frequency divided by two) to be present at the output. If the computer code is high (+5V), the input to nand gate 3 is low (0V) and the input to nand gate 5 is high (+5V). Again this permits the carrier (with frequency divided by one) to be present at the output. The result is FSK modulation. If the switch is closed, the circuit operates as described above except when the computer code is low (0V). With the switch closed there is no output from the modulator when the computer output is low (0V) which results in OOK modulation. The output of the modulator is then fed to the driver circuitry which drives the laser diode. The laser is then pulsed at the carrier frequency or carrier frequency divided by two depending upon the state of the computer output and the modulator switch position.

TABLE C-1

MICROPROCESSOR 8080 PROGRAM FOR CONTROLLING

TRANSMITTER TO TRANSMIT MILES CODE

ADDRESS		ASSEMBLY	OP CODE
3D00	Start	LXI SP, #3CF0	31F03C
3D03		LXI HL, #MES1	21D03E
3D06		CALL OUT	C0003E
3D09		MVI D, #9	1609
3D08		MVI B, #0	0600
3D0D	Start 1:	DCR D	15
3D0E		JZ Start 2	CA773D
3D11		CALL 1BC2	CD2B3E
3D14		JMP Start 1	C30D3D
3D17	Start 2:	MOV E,B	58
3D18		MVI B, #0	0600
3D1A		MVI D, #4	1604
3D1C	Start 3:	DCR D	15
3D1D		JZ Start 4	CA263D
3D20		CALL 1BC2	CD2B3E
3D23		JMP Start 3	C31C3D
3D26	Start 4:	LXI HL, #Temp 1	21F13C
3D29		MOV M,E	73
3D2A		INX H,L	23
3D2B		MOV M,B	70
3D2C	Start 5:	LXI HL, #MES2	21033F
3D2F		CALL OUT	CD003E

ADDRESS		ASSEMBLY	OP CODE
3D32		MVI E, 00	1E00
3D34		CALL DECB	CD333E
3D37		LXI #Temp 3	21F33C
3D3A		MOV M,E	73
3D3B	Start 6:	LXI HL, MES3	21313F
3D3E		CALL OUT	CD003E
3D41		CALL IN	CD0C3E
3D44		CPI #53	FE53
3D46		JNZ Start 6	C2003D
3D49		CALL SHIFT	CD7D3E
3D4C		CALL OUT 1	CD593E
3D4F		LXI HL, #MES4	21543F
3D52		CALL OUT	CD003E
3D55		JMP Start	C3003D
3E00	OUT:	MOV A,M	7E
3E01		CPI #00	FE00
3E03		RZ	C8
3E04		MOV C,A	4F
3E05		CALL 07FA	CDFA07
3E08		INX HL	23
3E09		JMP OUT	C3003E
3E0C	IN:	CALL 0729	CD2907
3E0F		MOV C,A	4F
3E10		CALL 07FA	CDFA07
3E13		ANI #7F	E67F

ADDRESS		ASSEMBLY	OP CODE
3E15		RET	C9
3E16	IBC:	CALL IN	CD0C3E
3E19		CPI #4D	FE49
3E1B		JZ #MISS	CA003D
3E1E		CPI #32	FE32
3E20		JNC #Start	D2003D
3E23		CPI #30	FE30
3E25		JC #Start	DA003D
3E28		ANI #1	E601
3E2A		RET	C9
3E2B	IBC2:	CALL IBC	CD163E
3E2E		RAR	IF
3E2F		MOV A,B	78
3E30		RAL	17
3E31		MOV B,A	47
3E32		RET	C9
3E33	DECB:	MVI D, #2	1602
3E35		PUSH DE	D5
3E36		LXI, D,0	110000
3E39	LOOP:	CALL IN	CD0C3E
3E3C		CPI #3A	FE3A
3E3E		JNC Start 5	D22C3D
3E41		CPI #30	FE30
3E43		JC Start 5	DA2C3D
3E46		ANI #0F	E60F

ADDRESS		ASSEMBLY	OP CODE
3E48		ADDE	83
3E49		NOV E,A	5F
3E4A		POP B,C	C1
3E4B		DCR B	05
3E4C		RZ	C8
3E4D		PUSH B	C5
3E4E		XCHG	EB
3E4F		DAD H,L	29
3E50		PUSH H,L	E5
3E51		DAD H,L	29
3E52		DAD H,L	29
3E53		POP B,C	C1
3E54		DAD B,C	09
3E55		XCHG	EB
3E56		JMP LOOP	C3393E
3E59	OUT 1:	LX1 HL, Temp 1	21F33C
3E5C		MOV C,M	4E
3E5D		LHLD Temp 1	2AF13C
3E60		XCHG	EB
3E61	OUT 2:	MOV H,E	63
3E62		MOV L,D	6A
3E63		MVI B, #B	060B
3E65		MOV A,H	7C
3E66		ANI #80	E680
3E68		RAL	17

ADDRESS		ASSEMBLY	OP CODE
3E69		RAL	17
3E6A		OUT E8	D3E8
3E6C		DAD H,L	29
3E6D		CALL DELAY	CD873E
3E70		MVI A,00	3E00
3E72		DCR B	05
3E73		JNZ OUT 3	C2653E
3E76		OUT E8	D3E8
3E78		DCR C	OD
3E79		JNZ OUT 2	C2613E
3E7C		RET	C9
3E7D	SHIFT:	LX1 HL, Temp 2	21F23C
3E80		MOV A,M	7E
3E81		RAR	1F
3E82		RAR	1F
3E83		RAR	1F
3E84		RAR	1F
3E85		MOV M,A	77
3E86		RET	C9
3E87	DELAY:	MVI A, #26	3E14
3E89	DELAY 1:	DCR A	3D
3E8A		JNZ DELAY	C2893E
3E8D		INC A	3C
3E83		INC A	3C
3E8F		MVI A, #14	3E14
3E91		RET	C9

ADDRESS		ASSEMBLY	OP CODE
3EDO	Message 1:	/CR LF Enter 11 Bit Character Code or M For Missiles? CR LF/	
3F03	Message 2:	/CR LF Enter The Number of Times To Repeat Code? CR LF/	
3F31	Message 3:	/CR LF Press S To Start Transmission. CR LF/	
3FS4	Message 4:	/CR LF Code Has Been Transmitted. CR LF/	

TABLE C-2
SYMBOL TABLE

MES 1	=	3EDO	TEMP 1	=	3CF1
MES 2	=	3F03	TEMP 2	=	3CF2
MES 3	=	3F31	TEMP 3	=	3CF3
MES 4	=	3F54	SHIFT	=	3E7D
START	=	3D00	IBC	=	3E16
START 1	=	3DOD	IBC 2	=	3E2B
START 2	=	3D17	DECB	=	3E33
START 3	=	3D1C	LOOP	=	3E39
START 4	=	3D26	OUT 1	=	3E59
START 5	=	3D2C	OUT 2	=	3E61
START 6	=	3D3B	OUT 3	=	3E65
OUT	=	3E00	DELAY	=	3E87
DELAY 1	=	3E88			

NOTE 1: 0729 is the address for the Prompt 80's input subroutine. (input one ASCII character)

NOTE 2: 07FA is the address for the Prompt 80's output subroutine. (output one ASCII character)

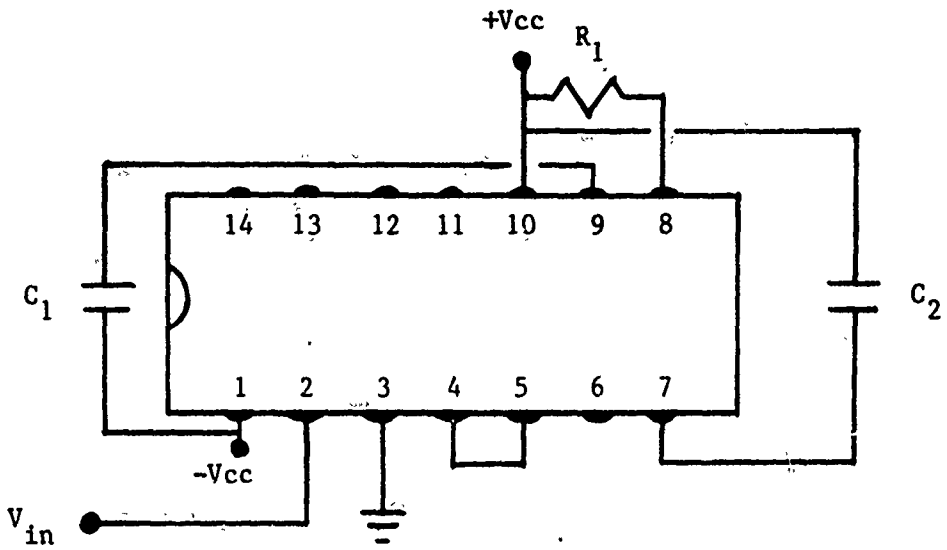

Fig. C-2. Circuit connections for PLL chip.

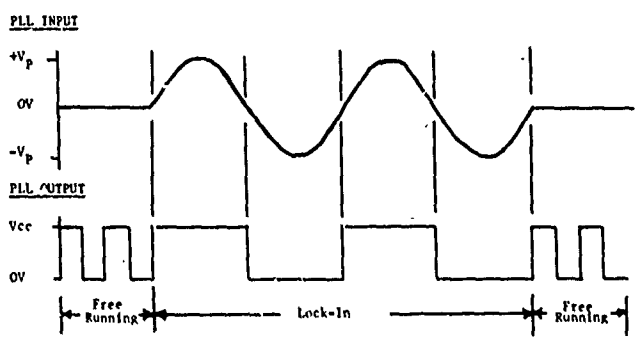

Fig. C-3. Output waveforms when PLL is locked onto signal and when it is free-running.

In order to check the computer program the Tektronix 7704 Digital Processing Oscilloscope and the Hewlett Packard 5333A frequency counter were used. To verify the program a code word of 10000000000 was entered and repeated indefinitely, which corresponded to a frequency of 273 Hz. The first bit was high for 332 μ sec leading to a corresponding word frequency of 271.1 Hz. This meant there was an error of 0.6% between the MILES and Prompt 80 code generators.

C.2 Receivers:

A. Phase Locked Loop (PPL):

A phase locked loop is an electronic feedback serve loop consisting of a phase detector, a low pass filter and a voltage controlled oscillator. The controlled phase of the oscillator makes this system capable of tracking and locking onto a received periodic signal. Even though the signal-to-noise ratio is very small, and thus almost lost in noise, the phase locked loop can lock-in on only a few cycles. Laboratory experiments with the 565 PLL chip is still one of the most versatile in many applications even though it is several years old. It has a bandwidth of 500 KHz, a center frequency stability of 1200 PPM/°C and a negligible frequency shift with drift of the supply voltage. A circuit diagram for the PLL chip used is shown in Fig. C-2. In the absence of signal, the VCO is free running since its frequency is determined by external components. Fig. C-3 shows the output of the PLL when the circuit is locked onto the received signal and also when there is no signal present. A filter follows the PLL in order to eliminate the free running PLL oscillator signal. The particular filter used in the laboratory experiments is shown in Fig. C-4. This blocking filter is followed by a comparator so as to return to an appropriate digital form of the signal. An active

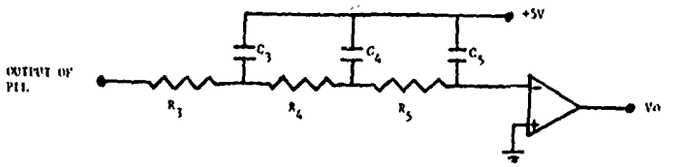

Fig. C-4. Filter used on output of PLL to allow modulated MILES signal to pass and block the free-running signal under the non-locked condition.

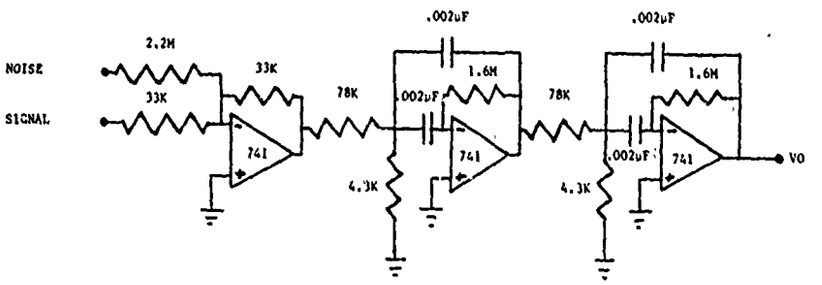

Fig. C-5. Active filter used in receiver to detect presence of high-pulse-rate modulated MILES codes.

filter could be used in place of the three stage passive filter shown in Fig. C-4.

B. Active Filter:

The Active Filter (AF) used for laboratory comparison with the PLL is shown in Fig. C-5. The gain of the op-amps was 10 and the Q was 10. The laboratory experiments made clear that a PLL is preferred to the AF for the following reasons:

1. The PLL reached lock-in in fewer pulses than the AF.

2. The PLL performed over a greater range of pulse rate drifting than did the AF.

Even with high performance op-amps in the AF, laboratory results suggested that the PLL performs more effectively.

REFERENCES

[1] V. I. Tartarski, Wave Propagation in a Turbulent Medium, McGraw-Hill Book Co., Inc. New York (1961), trans. by R. S. Silverman

[2] R. S. Lawrence and J. W. Strohbehn, "A survey of clear-air propagation effects relevant to optical communications," Proc. IEEE, vol. 58, No. 10, Oct. (1970),pp. 1523-1545

[3] D. A. DeWolf, "Strong irradiance fluctuations in turbulent air: plane waves," J. Opt. Soc. Amer., vol. 62 (1972), pp. 966-971

[4] D. A. DeWolf, "Waves in turbulent air: a phenomenological model," Proc. IEEE, vol. 62, No. 11, Nov. (1974), pp. 1523-1529

[5] S. F. Clifford, G. R. Ochs, and R. S. Lawrence, "Saturation of optical scintillations by strong turbulence," J. Opt. Soc. Amer., vol. 64, No. 2, Feb. (1974), pp. 148-154

[6] E. Jakeman and P. N. Pusey, "A model for non-Rayleigh sea echo," IEEE Trans. Antenn. and Prop., vol. AP-24, No. 6, Nov. (1976), pp. 806-814

[7] A. Ishimaru, "Theory and application of wave propagation and scattering in random media," Proc. IEEE, vol. 65, No. 7, July (1977), pp. 1030-1061

[8] J. K. Jao and M. Elbaum, "First-order statistics of a non-Rayleigh fading signal and its detection," Proc. IEEE, vol. 66, No. 7, July (1978), pp. 781-789

[9] G. Parry and P. N. Pusey, "K-distributions in atmospheric propagation of laser light," J. Opt. Soc. Amer., vol. 69, No. 5, May (1979), pp. 796-798

[10] G. R. Ochs, R. R. Bergman, and J. R. Snyder, J. Opt. Soc. Amer., vol. 59 (1969)

[11] J. R. Dunphy and J. R. Kerr, J. Opt. Soc. Amer., vol. 63 (1973)

[12] M. E. Gracheva, A. S. Gurvich, and M. A. Kallistratova, Izv. vuzov (Bull. Higher Ed. Inst.) Radiofizika (Radiophysics), vol. 13 (1970)

[13] T-I Wang and J. W. Strohbehn, "Perturbed log-normal distribution of irradiance fluctuations," J. Opt. Soc. Amer., vol. 64, No. 7, July (1974), pp. 994-1004

[14] F. Davidson and A. Gonzalez-del-Valle, "Measurements of three-parameter log-normally distributed optical-field irradiance fluctuations in a turbulent medium," J. Opt. Soc. Amer., vol. 65, No. 6, June (1975), pp. 655-663

[15] R. L. Fante, "Optical beam propagation in turbulent media," AFCRL-TR-75-0439, Phys. Sci. Res. Papers No. 640, Air Force Cambridge Res. Labs., Air Force Systems Command, USAF, Aug. (1975)

[16] M. Nakagami, "The m-distribution - A general formula of intensity distribution of rapid fading," reprint from Statistical Methods of Radio Wave Propagation, Pergamon Press (1960)

[17] M. Abramowitz and I. A. Stegun, eds., Handbook of Mathematical Functions, Nat. Bureau of Standards (1964)

[18] I. S. Gradshteyn and I. W. Ryzhik, Table of Integrals, Series, and Products, Academic Press, New York (1965)

[19] A. Erdelyi, et. al., Higher Transcendental Functions, Vol.'s 1 and 2, Bateman Manuscript Project, McGraw-Hill Book Co., New York (1953)

[20] J. Atchison and J. A. C. Brown, The Lognormal Distribution, Cambridge University Press, Cambridge (1957)

[21] Technical Report, Vol. I, Trainer Engineering Report (Final) for MILES, CDRL ITEM A002, XEOS Doc. No. 2350-AD-204, June (1980)